Hybrid Boundary Physics-Informed Neural Networks for Solving Navier-Stokes Equations with Complex Boundary

Chuyu Zhou*1, Tianyu Li*2, Chenxi Lan², Rongyu Du⁴, Guoguo Xin¹,+, Hangzhou Yang¹, Guoqing Wang²,++, Xun Liu³, Wei Li³,+++

¹School of Physics, Northwest University, Xi'an 710127, China

²School of Computer Science and Engineering, University of Electronic Science and Technology of China, Chengdu 611731, China

³Department of Imaging Technology, Beijing Institute of Space Mechanics and Electricity, Beijing 100094, China

⁴School of Information Science & Technology, Northwest University, Xi'an 710127, China ⁵Donghai Laboratory, Zhoushan, Zhejiang 316000, China

+xinguo@nwu.edu.cn
++qwang0420@hotmail.com
+++wei_li_bj@163.com

Abstract

Physics-informed neural networks (PINN) have achieved notable success in solving partial differential equations (PDE), yet solving the Navier-Stokes equations (NSE) with complex boundary conditions remains a challenging task. In this paper, we introduce a novel Hybrid Boundary PINN (HB-PINN) method that combines a pretrained network for efficient initialization with a boundary-constrained mechanism. The HB-PINN method features a primary network focused on inner domain points and a distance metric network that enhances predictions at the boundaries, ensuring accurate solutions for both boundary and interior regions. Comprehensive experiments have been conducted on the NSE under complex boundary conditions, including the 2D cylinder wake flow and the 2D blocked cavity flow with a segmented inlet. The proposed method achieves state-of-the-art (SOTA) performance on these benchmark scenarios, demonstrating significantly improved accuracy over existing PINN-based approaches.

1 Introduction

Fluid mechanics is an important field in science and engineering that deals with the study of the motion of liquids and gases. The NSE are basic partial differential equations that describe the dynamic behavior of viscous fluids, which are highly nonlinear partial differential equations and are widely used in aerodynamics, meteorology, oceanography, and industrial process simulations Munson et al. [1]. Although CFD methods have achieved considerable maturity, challenges such as mesh generation persist and can lead to numerical instability and reduced accuracy[2]. In recent years, PINNs, which integrate physical prior knowledge with deep learning [3], have emerged as a notable class of surrogate models for computational fluid dynamics.

PINN represent a deep learning methodology that incorporates physical constraints by embedding the governing physical equations and boundary conditions into the neural network's loss function. First proposed by Raissi et al. in 2019 [4], PINN eliminate the need for mesh generation, a requirement

inherent to traditional CFD solvers, while enabling more efficient resolution of inverse problems through data integration.

However, for fluid models with complex boundary conditions, conventional PINN methods often struggle to accurately approximate both the boundary conditions and the partial differential equations [5]. For conventional PINN, boundary conditions and initial conditions are explicitly embedded into the loss function, which is trained simultaneously with the PDE loss [4, 6]. A notable limitation of this loss formulation lies in its frequent failure to ensure simultaneous minimization of the PDE residual loss and the boundary condition loss. This issue becomes particularly pronounced when boundary conditions exhibit high complexity, thereby compromising the accuracy of the resultant solutions [7, 8, 9].

Here, to address the difficulty in balancing boundary condition losses and equation losses in complex boundary flow field problems, we propose a composite network approach specifically for complex boundary issues, named HB-PINN. By independently constructing a solution network that strictly enforces boundary conditions and a boundary-oriented distance function network, this method ensures applicability to diverse fluid dynamics problems with geometrically complex boundaries. To demonstrate the effectiveness of the proposed method, we conducted tests on two-dimensional incompressible flow fields under different boundary conditions, including steady-state and transient cases.

The main contributions of this work are as follows:

- 1. We propose a new PINN approach named HB-PINN that are embedded the boundary conditions to solve flow fields in regions with irregular obstructing structures.
- 2. A power function is proposed to refine the distance metric for handling complex boundary conditions, thereby improving prediction accuracy.
- 3. Extensive experimental validations on NSE with complex boundary conditions—such as the 2D cylinder wake problem and the 2D obstructed cavity flow with a segmented inlet—demonstrate the superior accuracy of the proposed model compared to existing PINN methods, thereby establishing new benchmarks.

2 Related Works

PINN methods for PDE. PINN were initially proposed by Raissi et al.[4]. The methods have been extended to diverse domains, including: fluid mechanics[10, 11], medical applications[12, 13], heat transfer[14, 15], and materials science[16, 17]. Furthermore, multiple PINN variants have been developed based on PINN, such as: Modified Fourier Network PINN (MFN-PINN)[18], hp-VPINN[19], Conservative PINN (CPINN)[20]. These variants enhance the generalizability and accuracy of PINN in solving heterogeneous PDE systems.

Loss conflict problems. The PINN framework explicitly embeds boundary and initial conditions into the loss function, and the resultant loss conflict problem has garnered significant attention from the research community. A pivotal development by Lu et al. (2021) [21] proposes a distance-informed ansatz that provably satisfies boundary conditions through analytically constructed solutions. This architecture enables exclusive optimization of PDE residuals during training. SA-PINN [22] proposes a spatially adaptive weight matrix to dynamically mitigate gradient conflicts between region-specific loss components during optimization. XPINN [23], as a generalized extension of PINN, introduces an interface-informed decomposition framework for solving nonlinear PDE on arbitrarily complex geometries. Although these methods show significant improvements in loss balancing compared to baseline PINN models, they still suffer from inaccuracies when handling problems with highly complex boundary conditions.

Complex boundary problems. Botarelli et al. [24] employed a Modified Fourier Network (MFN-PINN) to solve flow field problems with complex boundaries, demonstrating its superiority through comparisons with Multi-Layer Perceptron-based PINN (MLP-PINN). Sukumar et al. [25] proposed an R-function-based distance function construction method for enforcing boundary conditions in PINN, which significantly improves convenience in first-order derivative-dominated problems. However, the complex boundary analytical distance functions (ADF) constructed by R-functions are not natural functions.

To address the loss term conflicts induced by complex boundary conditions, this work decouples the boundary constraints into two sub-functions: a particular solution function that strictly enforces boundary conditions while being weakly trained on the governing equations, and a distance function describing the spatial proximity to boundaries. Furthermore, to ensure global differentiability of the distance function, we formulate it via a DNN architecture.

3 Methodology

3.1 Incompressible Navier-Stokes Equations

The incompressible Navier-Stokes equations, excluding external body forces, serve as the governing equations for all flow cases in this study, expressed as:

$$\nabla \cdot \mathbf{u} = 0, \quad \frac{\partial \mathbf{u}}{\partial t} + (\mathbf{u} \cdot \nabla) \mathbf{u} + \frac{1}{\rho} \nabla p - \nu \nabla^2 \mathbf{u} = 0. \tag{1}$$

In the equations, \mathbf{u} , p, ρ , and ν denote the velocity vector, fluid pressure, density and dynamic viscosity coefficients, respectively. For incompressible flows, ρ and ν are characteristic fluid parameters that remain spatially and temporally invariant.

3.2 HB-PINN Approach

The architecture of our proposed method is illustrated in Fig.1. The framework consists of three subnetworks: $\mathcal{N}_{\mathcal{P}}$, $\mathcal{N}_{\mathcal{D}}$, and $\mathcal{N}_{\mathcal{H}}$. The $\mathcal{N}_{\mathcal{P}}$ subnetwork (Particular Solution Network) is trained to satisfy boundary conditions, while the $\mathcal{N}_{\mathcal{D}}$ subnetwork (Distance Metric Network) learns boundary-condition-aware weights by encoding the distance from interior points to domain boundaries. The $\mathcal{N}_{\mathcal{H}}$ subnetwork (Primary Network) is dedicated to resolving the governing PDE. During the final training phase, only the parameters of $\mathcal{N}_{\mathcal{H}}$ are optimized, whereas $\mathcal{N}_{\mathcal{P}}$ and $\mathcal{N}_{\mathcal{D}}$ remain fixed as pre-trained components. This design effectively addresses challenges involving hybrid interior-exterior boundary configurations. Therefore, we term this methodology Hybrid Boundary Physics-Informed Neural Networks.

In our model, the constraints on the variables are formulated as follows:

$$q(\mathbf{x},t) = \mathcal{P}_q(\mathbf{x},t) + \mathcal{D}_q(\mathbf{x},t) \cdot \mathcal{H}_q(\mathbf{x},t), \tag{2}$$

here, $q(\cdot)$ denote the physical quantities of interest (e.g., u,v, and p in a 2D flow model); \mathcal{P}_q represents an additional solution function that satisfies the boundary conditions; \mathcal{D}_q is the distance function; \mathcal{H}_q is the output of the primary network. The distance function \mathcal{D}_q takes a value of 0 at the domain boundaries and rapidly increases to 1 as it moves away from the boundaries. Functionally, \mathcal{D}_q acts as a weight for \mathcal{H}_q , modulating its influence across the computational domain.

Under this formulation, the distance function \mathcal{D}_q enforces strict boundary condition compliance by evaluating to zero at domain boundaries while smoothly transitioning to \mathcal{H}_q , which satisfies the governing equations in interior regions. When boundary conditions and geometric configurations are simple, both \mathcal{P}_q and \mathcal{D}_q can be analytically expressed. However, analytical expressions for \mathcal{P}_q and \mathcal{D}_q are generally infeasible for complex geometries. Consequently, we leverage three dedicated deep neural networks (DNN), the previously defined $\mathcal{N}_{\mathcal{P}}$, $\mathcal{N}_{\mathcal{D}}$, and $\mathcal{N}_{\mathcal{H}}$, to parameterize these components. The composite solution for 2D incompressible flows is thus constructed as:

$$\mathcal{N}_{q}(\boldsymbol{x},t) = \mathcal{N}_{\mathcal{P}_{q}}(\boldsymbol{x},t) + \mathcal{N}_{\mathcal{D}_{q}}(\boldsymbol{x},t) \cdot \mathcal{N}_{\mathcal{H}_{u}}(\boldsymbol{x},t). \tag{3}$$

Sub-network $\mathcal{N}_{\mathcal{P}}$

The subnetwork $\mathcal{N}_{\mathcal{P}}$ adopts the same architecture as conventional PINN, with outputs comprising the velocity components u, v, and pressure p. The loss function for training $\mathcal{N}_{\mathcal{P}}$ is formulated by integrating residuals of the NSE, boundary conditions (BC), and initial conditions (IC), expressed as:

$$\mathcal{L} = \lambda_1 \mathcal{L}_{PDE} + \lambda_2 \mathcal{L}_{IC} + \lambda_3 \mathcal{L}_{BC}, \tag{4}$$

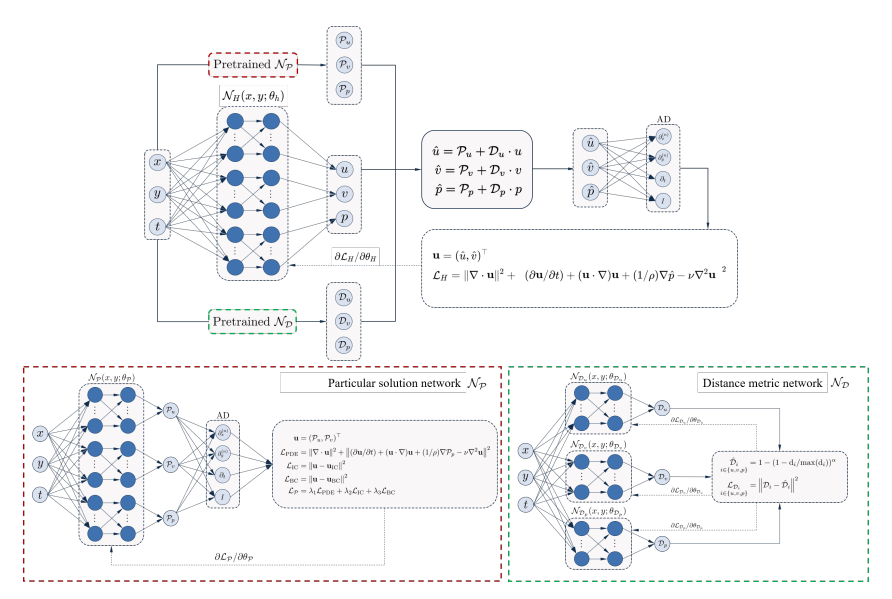


Figure 1: The architecture of the proposed method.

where

$$\mathcal{L}_{BC} = \frac{1}{N_{BC}} \sum_{i=1}^{N_{BC}} \|\mathbf{u}(x_i, t_i) - \mathbf{u}_{BC}(x_i, t_i)\|^2,$$
 (5)

$$\mathcal{L}_{IC} = \frac{1}{N_{IC}} \sum_{i=1}^{N_{IC}} \|\mathbf{u}(x_i, t_0) - \mathbf{u}_{IC}(x_i, t_0)\|^2,$$
(6)

and

$$\mathcal{L}_{PDE} = \frac{1}{N_{PDE}} \sum_{i=1}^{N_{PDE}} \left(\left\| \nabla \cdot \mathbf{u} \right\|^2 + \left\| \frac{\partial \mathbf{u}}{\partial t} + (\mathbf{u} \cdot \nabla) \mathbf{u} + \frac{1}{\rho} \nabla p - \nu \nabla^2 \mathbf{u} \right\|^2 \right). \tag{7}$$

Here, $\lambda_i (i=1,2,3)$ denote the loss weighting coefficients corresponding to each term. Adjusting these weights allows biasing the network's training dynamics to enhance solution accuracy. Our $\mathcal{N}_{\mathcal{P}}$ subnetwork prioritizes boundary and initial condition enforcement by assigning $\lambda_2, \lambda_3 \gg \lambda_1$ (e.g., $\lambda_1=1; \lambda_2, \lambda_3=1000$), enabling preliminary PDE training while strictly satisfying boundary constraints

By decoupling the training objectives, the subnetwork $\mathcal{N}_{\mathcal{P}}$ focuses exclusively on enforcing boundary conditions through loss weight modulation, without imposing strict constraints on governing equation residuals. This targeted approach circumvents the multi-loss balancing challenges inherent to conventional PINN, while delegating full PDE resolution to the primary network $\mathcal{N}_{\mathcal{H}}$.

Sub-network $\mathcal{N}_{\mathcal{D}}$

The $\mathcal{N}_{\mathcal{D}}$ subnetwork is a shallow DNN designed to construct distance functions. For each quantity q of interest, we introduce a distance metric network $\mathcal{N}_{\mathcal{D}_q}$. To train this network, sampling points (x,t) are firstly collected from the space-time domain $\Omega \times [0,T]$. The network is then supervised to approximate the signed distance function $\hat{\mathcal{D}}_q(x,t)$ between these points and the boundary associated with q, formulated as:

$$\hat{\mathcal{D}}_q = \min(\text{distance to the spatiotemporal boundary of } q). \tag{8}$$

In order to ensure the network outputs approach 0 near domain boundaries and rapidly increase to 1 in regions far from boundaries, while maintaining dominance of the primary network $\mathcal{N}_{\mathcal{H}_q}$'s predictions in interior regions, we employ a power-law function $f(\hat{\mathcal{D}}_q)$ derived from the distance metric $\hat{\mathcal{D}}_q$ as the training labels for the subnetwork $\mathcal{N}_{\mathcal{D}_q}$. The power-law function $f(\hat{\mathcal{D}}_q)$ is defined as follows:

$$f(\hat{D}_q) = 1 - (1 - \hat{D}_q / \max(\hat{D}_q))^{\alpha}.$$
 (9)

The parameter α is a positive value controlling the growth rate of the function. The curves exhibit steeper gradients near boundaries and smoother transitions in regions distant from boundaries. Larger α values enhance the sensitivity of the distance metric network to boundary-proximal points while diminishing its response to interior points, thereby reducing computational demands. However, excessively large α values may lead to erroneous predictions of near-boundary points as having distance values close to 1, which undermines the influence of the specialized solution network in critical regions. To accommodate varying boundary complexities across models, α can be tuned to maintain the steepness of the power-law function within a reasonable range. The loss function for the distance metric network is defined as:

$$\mathcal{L}_{\mathcal{D}_q} = \frac{1}{N_{\mathcal{D}_q}} \sum_{i=1}^{N_{\mathcal{D}_q}} \| \mathcal{D}_q - f\left(\hat{\mathcal{D}}_q\right) \|^2.$$
 (10)

Here, \mathcal{D}_q represents the network's output, supervised by the training labels $f(\hat{\mathcal{D}}_q)$. This approach ensures robust training of $\mathcal{N}_{\mathcal{D}_q}$ even under highly complex boundary conditions, while simultaneously enhancing the accuracy of the primary network's training outcomes.

Sub-network $\mathcal{N}_{\mathcal{H}}$

The $\mathcal{N}_{\mathcal{H}}$ subnetwork also employs a DNN architecture but with a larger scale compared to the $\mathcal{N}_{\mathcal{P}}$ and $\mathcal{N}_{\mathcal{D}}$ subnetworks. Through pre-training of the $\mathcal{N}_{\mathcal{P}}$ and $\mathcal{N}_{\mathcal{D}}$ subnetworks, boundary conditions are strictly enforced, allowing $\mathcal{N}_{\mathcal{H}}$ to focus solely on minimizing the governing equation residuals. For the 2D incompressible NSE, the loss function of the $\mathcal{N}_{\mathcal{H}}$ subnetwork is defined as:

$$\mathcal{L}_{\mathcal{H}} = \frac{1}{N_{\text{PDE}}} \sum_{i=1}^{N_{\text{PDE}}} \left(\|\nabla \cdot \hat{\mathbf{u}}\|^2 + \left\| \frac{\partial \hat{\mathbf{u}}}{\partial t} + \hat{\mathbf{u}} \cdot \nabla \hat{\mathbf{u}} + \frac{1}{\rho} \nabla \hat{p} - \nu \nabla^2 \hat{\mathbf{u}} \right\|^2 \right). \tag{11}$$

While this formulation shares the same structure as Eq.7, the variables $\hat{\mathbf{u}}$ and \hat{p} are derived from the modified outputs of Eq.2. This training strategy enables the $\mathcal{N}_{\mathcal{H}}$ subnetwork to focus exclusively on PDE compliance during optimization, effectively eliminating the conflicting gradients between equation residuals and boundary condition losses that commonly plague conventional PINN.

4 Experiments

To evaluate the effectiveness of the proposed approach, three two-dimensional incompressible flow cases are investigated, including two steady-state cases and one transient case, to demonstrate the general applicability of our method across different flow fields.

The steady-state and transient incompressible Navier-Stokes equations were solved via the finite element method (FEM), with mesh density ensuring solution accuracy and numerical stability. A time step size of $\Delta t = 0.01$ was adopted for transient simulations. The CFD results obtained under these configurations were utilized as ground truth (GT), the proposed HB-PINN is benchmarked against the conventional soft-constrained PINN (sPINN) [4], hard-constrained PINN (hPINN) [21], modified Fourier Network PINN (MFN-PINN) [18, 24], extended PINN (XPINN) [23], self-adaptive PINN (SA-PINN) [22], and PirateNets [26]. Notably, the hPINN, proposed by Lu et al.[21], exhibits erratic behavior in scenarios with complex boundary conditions, often failing to produce reliable results for comparative analysis. To ensure comparability of results, the comparative analysis of the hPINN method in this study selectively relaxes the enforcement of boundary conditions in specific subdomains, as exemplified by the near-inlet wall regions in Case 2 (0 < x < 0.4, y = 0 & y = 1). The detailed rationale for relaxing boundary conditions is provided in Appendix D. Additionally, to

assess the impact of our HB-PINN, we conducted three ablation studies on Case 2, the results are provided in Appendix C.

In this section, the experimental setup is introduced first, followed by three case studies: steady-state two-dimensional flow around a cylinder, steady-state flow in a segmented inlet with an obstructed square cavity, and transient flow in a segmented inlet with an obstructed square cavity.

4.1 Experimental Settings

As illustrated in Fig. 1, the proposed HB-PINN takes space-time coordinates as inputs and outputs velocity components (u, v) and pressure p. In the implementation phase, the training process employs a distributed architecture: each subnetwork $(\mathcal{N}_{\mathcal{P}}, \mathcal{N}_{\mathcal{D}}, \text{ and } \mathcal{N}_{\mathcal{H}})$ utilizes three independent DNN dedicated to variables u, v, and p, resulting in a total of nine distinct DNN. After obtaining separate predictions for u, v, and p, these outputs are integrated through Eq. 3 to reconstruct the composite solution. For detailed training protocols refer to Appendix B.

In the models discussed in this study, the NSE are non-dimensionalized using characteristic scales. For the three benchmark cases analyzed in the main text, the Reynolds number is uniformly set to Re=100 as the baseline configuration. Comparative studies at higher Reynolds numbers (Re=500,1000,2000) are systematically documented in Appendix E.

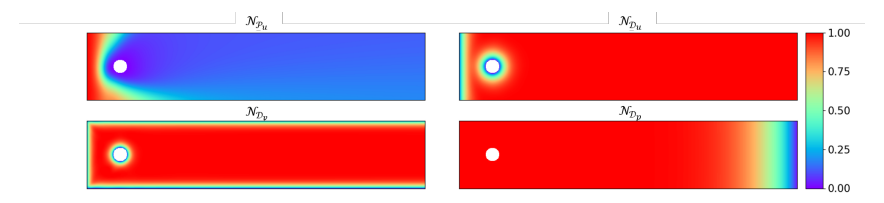


Figure 2: The trained boundary prediction for the Case 1. $\mathcal{N}_{\mathcal{P}_u}$ represents the result of the particular solution network for u, while $\mathcal{N}_{\mathcal{D}_u}$, $\mathcal{N}_{\mathcal{D}_v}$, and $\mathcal{N}_{\mathcal{D}_p}$ respectively represent the results of the distance metric network for u, v, and p.

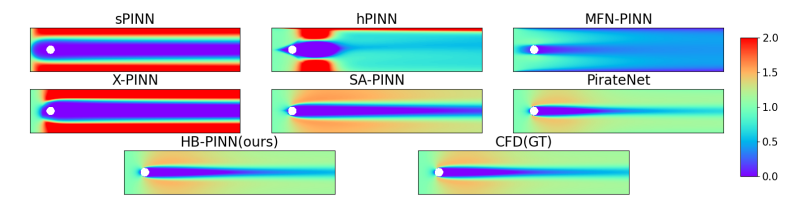


Figure 3: Velocity distributions for the flow around a cylinder from different methods.

4.2 Case 1: Two-dimensional flow around a cylinder

The flow past a circular cylinder represents a canonical benchmark in fluid mechanics(see Appendix A.1 for detailed geometric specifications). The boundary conditions are specified as follows:

$$\label{eq:sum_eq} \begin{split} u &= 1, \quad x = 0, \; 0 \leq y \leq 1; \qquad u \cdot n_x = 0, \quad \text{others}; \\ v \cdot n_y &= 0, \quad \text{on } \partial \Omega; \qquad \qquad p = 0, \quad x = 5, \; 0 \leq y \leq 1. \end{split}$$

Following Eq.4, the loss function for the $\mathcal{N}_{\mathcal{P}}$ subnetwork in the proposed model is formulated as:

$$\begin{split} \mathcal{L}_{\mathcal{P}} = & \lambda_{1} \Big(\left\| \nabla \cdot \hat{u} \right\|^{2} + \left\| \partial \hat{u} / \partial t + \left(\hat{u} \cdot \nabla \right) \hat{u} + 1 / \rho \nabla \hat{p} - \\ & \nu \nabla^{2} \hat{u} \right\|_{x \in \Omega}^{2} \Big) + \lambda_{2} \left(\left\| \mathcal{U}_{\mathcal{P}} - \mathcal{U}_{B} \right\|_{x \in \partial \Omega}^{2} + \left\| p_{\mathcal{P}} - p_{B} \right\|_{x \in \partial \Omega}^{2} \right). \end{split}$$

Here, Ω denotes the interior of the geometric region, while $\partial\Omega$ denotes the boundary. The loss weight λ_1 for the equation part is set to 1, and the loss weight λ_2 for the boundary part is set to 1000, with the aim of making the network focus more on the training of boundary conditions.

The outputs of the $\mathcal{N}_{\mathcal{P}}$ and $\mathcal{N}_{\mathcal{D}}$ networks are shown in Fig.2. The final modification to the variable result is as follows:

$$\hat{u} = \mathcal{N}_{\mathcal{P}_u}(x,t) + \mathcal{N}_{\mathcal{D}_u}(x,t) \cdot \mathcal{N}_{\mathcal{H}_u}(x,t), \hat{v} = \mathcal{N}_{\mathcal{D}_v}(x,t) \cdot \mathcal{N}_{\mathcal{H}_v}(x,t), \text{ and } \hat{p} = \mathcal{N}_{\mathcal{D}_p}(x,t) \cdot \mathcal{N}_{\mathcal{H}_p}(x,t).$$

Since both v and p are set to 0 at the boundary, there is no need to configure the boundary results separately; they are simply constrained by the distance function.

In the case of 2D cylindrical pipe flow model, the qualitative results from sPINN, hPINN, MFN-PINN, XPINN, SA-PINN, PirateNet, HB-PINN are shown in Fig.3. The residuals of these methods compared with CFD results are shown in Fig.4. More detailed error metrics are summarized in the "Case1" section of Table 1.

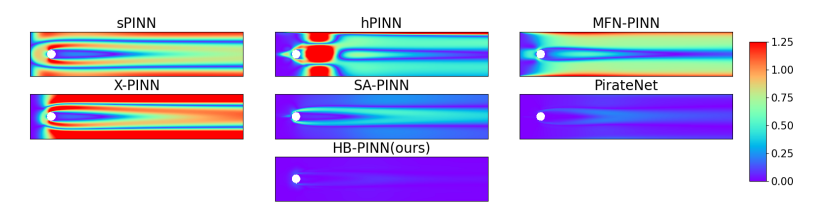


Figure 4: The residuals of sPINN, hPINN, MFN-PINN, XPINN, SA-PINN, PirateNet, and our HB-PINN compared to the GT in Case 1.

4.3 Case 2: steady-state flow in a segmented inlet with an obstructed square cavity

The model incorporates two rectangular obstructions positioned along the top and bottom walls of a square cavity, with a segmented inlet configuration (see Appendix A.2 for detailed geometric specifications). The boundary conditions are configured as follows:

$$u=0.5, \quad x=0, \ y\in [0,0.2]\cup [0.4,0.6]\cup [0.8,1]; \quad u=0, \ \text{others}; \ v=0, \ \text{on} \ \partial\Omega; \quad p=0, \ x=1, \ y\in [0.8,1].$$

The output results of the boundary condition solution function network related to u and the distance function network for u, v, and p are shown in Fig.5.

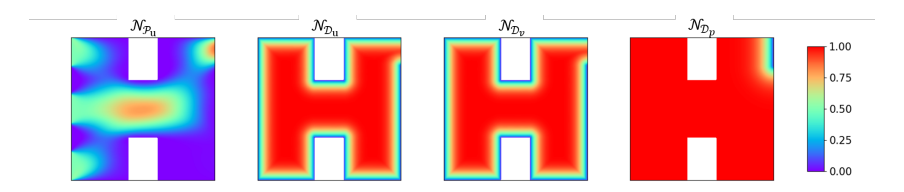


Figure 5: The trained boundary prediction for Case 2. \mathcal{N}_{P_u} represents the result of the particular solution network for u, while \mathcal{N}_{D_u} , \mathcal{N}_{D_v} , and \mathcal{N}_{D_p} respectively represent the results of the distance metric network for u, v, and p.

The velocity distributions for case 2 from sPINN, hPINN, MFN-PINN, SA-PINN, XPINN, PirateNet and our HB-PINN are shown in Fig.6. Compared to existing methods, the HB-PINN framework demonstrates superior capability in simulating models with complex inflow boundary conditions, achieving a MSE reduction of an order of magnitude relative to CFD benchmarks. The residuals of these methods compared with CFD results are shown in Fig. 7. More detailed error metrics are summarized in the "Case2" section of Table 1.

Based on Case 2, we conduct ablation studies on two critical pre-trained sub-networks by evaluating the outcomes of separately employing the specific solution network and the distance metric network. Here, "mP" denotes using only the particular solution network, while "mD" refers to using only the distance metric network.

Under the mP approach, the distance function is normalized solely based on the distance to the boundary without adjustment using power functions, resulting in lower accuracy within the domain. Under the mD approach, while internal errors are reduced during training, the enforcement of

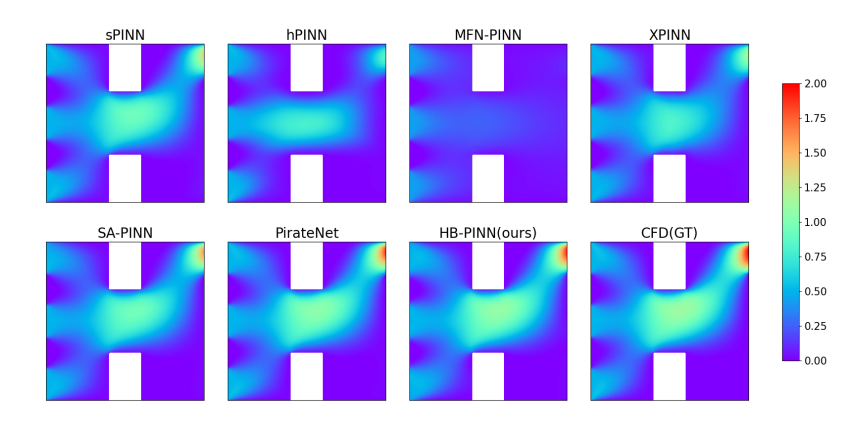


Figure 6: Comparison of velocity distributions for Case 2 across different methods.

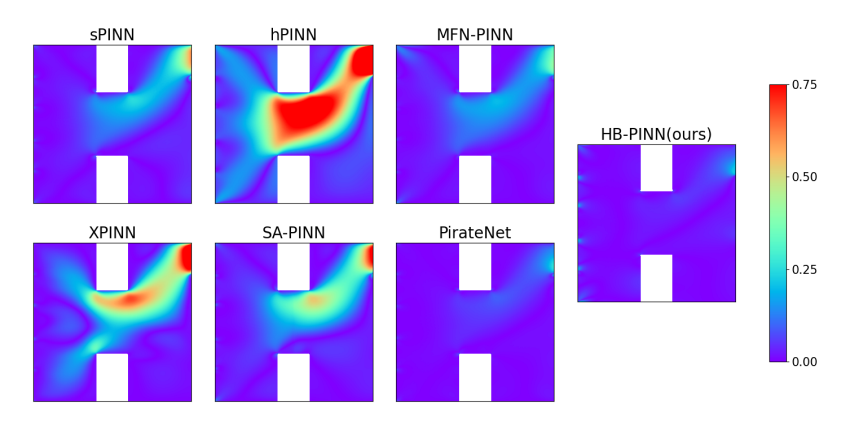


Figure 7: The residuals of sPINN, hPINN, MFN-PINN, XPINN, SA-PINN, PirateNet, and our HB-PINN compared to the GT in Case 2.

boundary conditions is imprecise, which affects the final results. These tests demonstrate that both constructive functions in our method contribute positively to the solution process, further validating the necessity of applying both functions simultaneously. The comparison of residuals is shown in Fig.8. For a more detailed error analysis, please refer to Table2 in Appendix C.

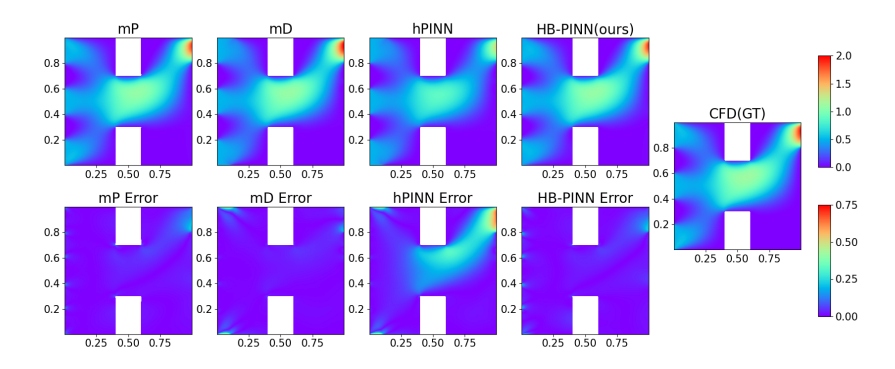


Figure 8: Comparison of velocity results and residuals between the mP and mD methods in Case 2.

4.4 Case 3: transient flow in a segmented inlet with an obstructed square cavity

The difference between this model and case 2 lies in the consideration of the transient situation, which further increases the complexity of the boundary conditions. The boundary conditions are set

as follows: the inlet normal velocity u is 0.5, the outlet static pressure is 0, and the velocity at other boundaries is set to 0, satisfying the no-slip condition. The initial conditions are set with the velocity components u, v and the pressure p all equal to 0. Relative to Case 2, the addition of initial conditions:

$$u = 0, v = 0, p = 0, \quad t = 0$$

The network structure parameters chosen for the transient case are the same as those for case 2. Fig. 9 shows the velocity results obtained using different methods at t=1. In the transient case, due to the increased complexity of the boundary conditions, the accuracy of the other methods significantly decreases, while HB-PINN maintains a high level of accuracy. The velocity results and the error compared to the CFD method are shown in Fig. 10. These results demonstrate the versatility of HB-PINN in both steady-state and transient situations.

Table 1: Comparative analysis of error metrics across three Cases. Among the baseline methods, PirateNet achieves the highest accuracy, while HB-PINN represents our proposed methodology.

Case	Method	Error Metrics			
Cusc	Wiedlod	MSE(↓)	MAE(↓)	Relative L2(↓)	
	sPINN	0.52078	0.64216	0.66805	
	hPINN	0.58347	0.52729	0.70712	
	MFN-PINN	0.42373	0.57410	0.21363	
Case 1	XPINN	1.11924	0.90927	0.97936	
	SA-PINN	0.05325	0.18967	0.21363	
	PirateNet	0.00763	0.06689	0.08089	
	HB-PINN	$\overline{0.00433}$	0.02012	0.06093	
	sPINN	0.008 01	0.05173	0.20036	
	hPINN	0.04060	0.11242	0.45110	
	MFN-PINN	0.11626	0.21186	0.76337	
Case 2	XPINN	0.02149	0.08385	0.32824	
	SA-PINN	0.00542	0.04580	0.16495	
	PirateNet	0.00186	0.02357	0.09679	
	HB-PINN	$\overline{0.00088}$	0.01888	0.06655	
	sPINN	0.124 00	0.21876	0.788 19	
Case 3	hPINN	0.15559	0.23951	0.88288	
	MFN-PINN	0.10543	0.20150	0.72678	
	XPINN	0.04149	0.12028	0.45592	
	SA-PINN	0.10612	0.19642	0.72915	
	PirateNet	0.03202	0.10682	0.40054	
	HB-PINN	0.00825	0.04870	0.20332	

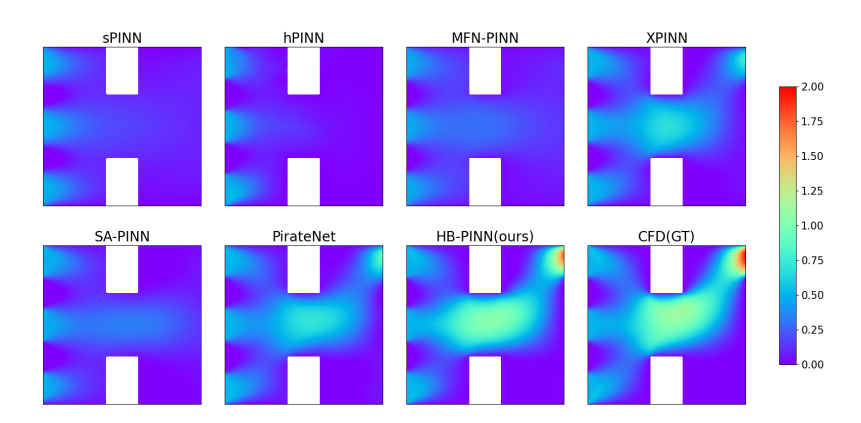


Figure 9: Comparison of velocity distributions at t = 1 for different methods in Case 3.

4.5 Result Discussion

The quantitative results of the error metrics between CFD calculation and the predictions from sPINN, hPINN, MFN-PINN, SA-PINN, XPINN, PirateNet and HB-PINN for the three cases are presented in Table 1. Combined with the qualitative results shown in Fig.3,4,6,7,9,10, it is shown that our HB-PINN can accurately solve complex boundary flow problems with interior barriers, while the traditional soft-constrained PINN (sPINN) method and hard-constrained PINN (hPINN) method incur significant errors in solving such problems. The training results of SA-PINN and XPINN show improvements in accuracy; however, significant errors persist in the cases with more complex boundary conditions.

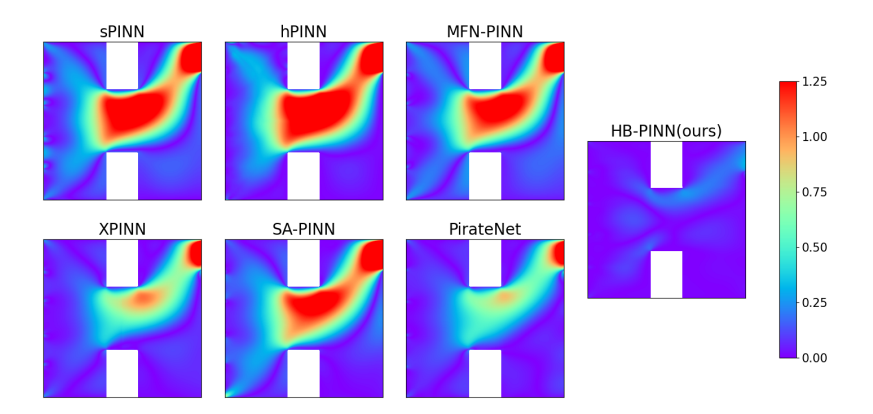


Figure 10: The residuals of sPINN, hPINN, MFN-PINN, XPINN, SA-PINN, PirateNet, and our HB-PINN compared to the GT in Case 3.

5 Limitations

The optimal values of critical parameters in the methodology, such as the α parameter in the distance metric network and the training iterations of the particular solution network, are currently determined empirically. Further research is required to systematically identify their optimal configurations.

6 Conclusion

PINN hold great potential as surrogate models for fluid dynamics; however, their application is often hindered by the complexity of the NSEs and intricate boundary conditions. This paper introduces a novel method, HB-PINN, which features a primary network focused on inner domain points and a distance metric network that enhances predictions at the boundaries, ensuring accurate solutions for both boundary and interior regions. This makes the approach applicable to be adaptable to more complex fluid dynamics models. Through tests on steady-state two-dimensional flow around a cylinder, steady-state segmented inlet with obstructed square cavity flow, and transient segmented inlet with obstructed square cavity flow, our method outperforms typical PINN approaches by a large margin, establishing itself as a benchmark for solving NSEs with complex boundaries. Additional analysis is provided in the appendices to further illustrate the effectiveness of our method.

Acknowledgements

The authors would like to acknowledge the financial support received from Donghai Laboratory (2024SSYS0091), Open Fund of Beijing Key Laboratory of Advanced Optical Remote Sensing Technology (AORS202408), National Natural Science Foundation of China (12304346), Development Program of the Department of Science and Technology of Shaanxi Province (2025CY-YBXM-073), and Haina Plan of Zhouchuang Future from Mei Lin.

References

- [1] B. R. Munson, D. F. Young, T. Okiishi, Sharon Hollars, and Katie Johnson. *Fundamentals of Fluid Mechanics*, page 53–84. WORLD SCIENTIFIC, Apr 2006.
- [2] A. McLay. Computational fluid dynamics: the basics with applications. *The Aeronautical Journal*, 100(998):365–365, 1996.
- [3] Yann LeCun, Yoshua Bengio, and Geoffrey Hinton. Deep learning. *Nature*, 521(7553):436–444, May 2015.
- [4] M. Raissi, P. Perdikaris, and G.E. Karniadakis. Physics-informed neural networks: A deep learning framework for solving forward and inverse problems involving nonlinear partial differential equations. *Journal of Computational Physics*, 378:686–707, Feb 2019.
- [5] Tsung-Yeh Hsieh and Tsung-Hui Huang. A multiscale stabilized physics informed neural networks with weakly imposed boundary conditions transfer learning method for modeling advection dominated flow. *Engineering with Computers*, May 2024.
- [6] M. Lai, Yongcun Song, Xiaoming Yuan, Hangrui Yue, and Tianyou Zeng. The hard-constraint pinns for interface optimal control problems. *arXiv.org*, 2023.
- [7] Salvatore Cuomo, Vincenzo Schiano Di Cola, Fabio Giampaolo, Gianluigi Rozza, Maziar Raissi, and Francesco Piccialli. Scientific machine learning through physics—informed neural networks: Where we are and what's next. *Journal of Scientific Computing*, 92(3), Jul 2022.
- [8] Jinshuai Bai, Timon Rabczuk, Ashish Gupta, Laith Alzubaidi, and Yuantong Gu. A physics-informed neural network technique based on a modified loss function for computational 2d and 3d solid mechanics. *Computational Mechanics*, Nov 2022.
- [9] Rafael Bischof and M. Kraus. Multi-objective loss balancing for physics-informed deep learning. *arXiv.org*, 2021.
- [10] Shengze Cai, Zhiping Mao, Zhicheng Wang, Minglang Yin, and George Em Karniadakis. Physics-informed neural networks (pinns) for fluid mechanics: a review. *Acta Mechanica Sinica*, 37(12):1727–1738, Dec 2021.
- [11] Luning Sun, Han Gao, Shaowu Pan, and Jian-Xun Wang. Surrogate modeling for fluid flows based on physics-constrained deep learning without simulation data. *Computer Methods in Applied Mechanics and Engineering*, 361:112732, 2020.
- [12] Francisco Sahli Costabal, Yibo Yang, Paris Perdikaris, Daniel E Hurtado, and Ellen Kuhl. Physics-informed neural networks for cardiac activation mapping. *Frontiers in Physics*, 8:42, 2020.
- [13] Mohammad Sarabian, Hessam Babaee, and Kaveh Laksari. Physics-informed neural networks for brain hemodynamic predictions using medical imaging. *IEEE transactions on medical imaging*, 41(9):2285–2303, 2022.
- [14] Shengze Cai, Zhicheng Wang, Sifan Wang, Paris Perdikaris, and George Em Karniadakis. Physics-informed neural networks for heat transfer problems. *Journal of Heat Transfer*, 143(6): 060801, 2021.
- [15] Navid Zobeiry and Keith D Humfeld. A physics-informed machine learning approach for solving heat transfer equation in advanced manufacturing and engineering applications. *Engineering Applications of Artificial Intelligence*, 101:104232, 2021.
- [16] Enrui Zhang, Ming Dao, George Em Karniadakis, and Subra Suresh. Analyses of internal structures and defects in materials using physics-informed neural networks. *Science advances*, 8(7):eabk0644, 2022.
- [17] Khemraj Shukla, Ameya D Jagtap, James L Blackshire, Daniel Sparkman, and George Em Karniadakis. A physics-informed neural network for quantifying the microstructural properties of polycrystalline nickel using ultrasound data: A promising approach for solving inverse problems. *IEEE Signal Processing Magazine*, 39(1):68–77, 2021.

- [18] Matthew Tancik, Pratul Srinivasan, Ben Mildenhall, Sara Fridovich-Keil, Nithin Raghavan, Utkarsh Singhal, Ravi Ramamoorthi, Jonathan Barron, and Ren Ng. Fourier features let networks learn high frequency functions in low dimensional domains. *Advances in neural information processing systems*, 33:7537–7547, 2020.
- [19] Ehsan Kharazmi, Zhongqiang Zhang, and George Em Karniadakis. hp-vpinns: Variational physics-informed neural networks with domain decomposition. *Computer Methods in Applied Mechanics and Engineering*, 374:113547, 2021.
- [20] Ameya D Jagtap, Ehsan Kharazmi, and George Em Karniadakis. Conservative physics-informed neural networks on discrete domains for conservation laws: Applications to forward and inverse problems. Computer Methods in Applied Mechanics and Engineering, 365:113028, 2020.
- [21] Lu Lu, Raphaël Pestourie, Wenjie Yao, Zhicheng Wang, Francesc Verdugo, and Steven G. Johnson. Physics-informed neural networks with hard constraints for inverse design. *SIAM Journal on Scientific Computing*, 43(6):B1105–B1132, Jan 2021.
- [22] Levi D. McClenny and Ulisses M. Braga-Neto. Self-adaptive physics-informed neural networks. *Journal of Computational Physics*, 474:111722, 2023. ISSN 0021-9991.
- [23] Ameya D. Jagtap and George Em Karniadakis. Extended physics-informed neural networks (xpinns): A generalized space-time domain decomposition based deep learning framework for nonlinear partial differential equations. *Communications in Computational Physics*, 28(5), 2020.
- [24] Tommaso Botarelli, Marco Fanfani, Paolo Nesi, and Lorenzo Pinelli. Using physics-informed neural networks for solving navier-stokes equations in fluid dynamic complex scenarios. *Engi*neering Applications of Artificial Intelligence, 148:110347, 2025. ISSN 0952-1976.
- [25] N. Sukumar and Ankit Srivastava. Exact imposition of boundary conditions with distance functions in physics-informed deep neural networks. *Computer Methods in Applied Mechanics* and Engineering, 389:114333, 2022. ISSN 0045-7825.
- [26] Sifan Wang, Bowen Li, Yuhan Chen, and Paris Perdikaris. Piratenets: Physics-informed deep learning with residual adaptive networks. *Journal of Machine Learning Research*, 25(402): 1–51, 2024.

NeurIPS Paper Checklist

1. Claims

Question: Do the main claims made in the abstract and introduction accurately reflect the paper's contributions and scope?

Answer: [Yes]

Justification: The abstract and introduction address the challenges encountered in modeling complex-boundary systems, systematically analyze their underlying causes, and demonstrate enhanced predictive accuracy in such scenarios through the proposed methodology.

Guidelines:

- The answer NA means that the abstract and introduction do not include the claims made in the paper.
- The abstract and/or introduction should clearly state the claims made, including the
 contributions made in the paper and important assumptions and limitations. A No or
 NA answer to this question will not be perceived well by the reviewers.
- The claims made should match theoretical and experimental results, and reflect how much the results can be expected to generalize to other settings.
- It is fine to include aspirational goals as motivation as long as it is clear that these goals are not attained by the paper.

2. Limitations

Question: Does the paper discuss the limitations of the work performed by the authors?

Answer: [Yes]

Justification: The conclusion and supplementary materials explicitly address the current limitations of the proposed methodology.

Guidelines:

- The answer NA means that the paper has no limitation while the answer No means that the paper has limitations, but those are not discussed in the paper.
- The authors are encouraged to create a separate "Limitations" section in their paper.
- The paper should point out any strong assumptions and how robust the results are to violations of these assumptions (e.g., independence assumptions, noiseless settings, model well-specification, asymptotic approximations only holding locally). The authors should reflect on how these assumptions might be violated in practice and what the implications would be.
- The authors should reflect on the scope of the claims made, e.g., if the approach was only tested on a few datasets or with a few runs. In general, empirical results often depend on implicit assumptions, which should be articulated.
- The authors should reflect on the factors that influence the performance of the approach. For example, a facial recognition algorithm may perform poorly when image resolution is low or images are taken in low lighting. Or a speech-to-text system might not be used reliably to provide closed captions for online lectures because it fails to handle technical jargon.
- The authors should discuss the computational efficiency of the proposed algorithms and how they scale with dataset size.
- If applicable, the authors should discuss possible limitations of their approach to address problems of privacy and fairness.
- While the authors might fear that complete honesty about limitations might be used by reviewers as grounds for rejection, a worse outcome might be that reviewers discover limitations that aren't acknowledged in the paper. The authors should use their best judgment and recognize that individual actions in favor of transparency play an important role in developing norms that preserve the integrity of the community. Reviewers will be specifically instructed to not penalize honesty concerning limitations.

3. Theory assumptions and proofs

Question: For each theoretical result, does the paper provide the full set of assumptions and a complete (and correct) proof?

Answer: [Yes]

Justification: For all theoretical constructs mentioned, complete assumptions and complete proofs are provided.

Guidelines:

- The answer NA means that the paper does not include theoretical results.
- All the theorems, formulas, and proofs in the paper should be numbered and crossreferenced.
- All assumptions should be clearly stated or referenced in the statement of any theorems.
- The proofs can either appear in the main paper or the supplemental material, but if they appear in the supplemental material, the authors are encouraged to provide a short proof sketch to provide intuition.
- Inversely, any informal proof provided in the core of the paper should be complemented by formal proofs provided in appendix or supplemental material.
- Theorems and Lemmas that the proof relies upon should be properly referenced.

4. Experimental result reproducibility

Question: Does the paper fully disclose all the information needed to reproduce the main experimental results of the paper to the extent that it affects the main claims and/or conclusions of the paper (regardless of whether the code and data are provided or not)?

Answer: [Yes]

Justification: The architecture of the framework is elaborated in Section 3, while comprehensive training details are provided in Appendix B.

Guidelines:

- The answer NA means that the paper does not include experiments.
- If the paper includes experiments, a No answer to this question will not be perceived well by the reviewers: Making the paper reproducible is important, regardless of whether the code and data are provided or not.
- If the contribution is a dataset and/or model, the authors should describe the steps taken to make their results reproducible or verifiable.
- Depending on the contribution, reproducibility can be accomplished in various ways. For example, if the contribution is a novel architecture, describing the architecture fully might suffice, or if the contribution is a specific model and empirical evaluation, it may be necessary to either make it possible for others to replicate the model with the same dataset, or provide access to the model. In general, releasing code and data is often one good way to accomplish this, but reproducibility can also be provided via detailed instructions for how to replicate the results, access to a hosted model (e.g., in the case of a large language model), releasing of a model checkpoint, or other means that are appropriate to the research performed.
- While NeurIPS does not require releasing code, the conference does require all submissions to provide some reasonable avenue for reproducibility, which may depend on the nature of the contribution. For example
 - (a) If the contribution is primarily a new algorithm, the paper should make it clear how to reproduce that algorithm.
- (b) If the contribution is primarily a new model architecture, the paper should describe the architecture clearly and fully.
- (c) If the contribution is a new model (e.g., a large language model), then there should either be a way to access this model for reproducing the results or a way to reproduce the model (e.g., with an open-source dataset or instructions for how to construct the dataset).
- (d) We recognize that reproducibility may be tricky in some cases, in which case authors are welcome to describe the particular way they provide for reproducibility. In the case of closed-source models, it may be that access to the model is limited in some way (e.g., to registered users), but it should be possible for other researchers to have some path to reproducing or verifying the results.

5. Open access to data and code

Question: Does the paper provide open access to the data and code, with sufficient instructions to faithfully reproduce the main experimental results, as described in supplemental material?

Answer: [No]

Justification: The source code is not currently open-sourced but will be made publicly available after further organization in future work.

Guidelines:

- The answer NA means that paper does not include experiments requiring code.
- Please see the NeurIPS code and data submission guidelines (https://nips.cc/public/guides/CodeSubmissionPolicy) for more details.
- While we encourage the release of code and data, we understand that this might not be possible, so "No" is an acceptable answer. Papers cannot be rejected simply for not including code, unless this is central to the contribution (e.g., for a new open-source benchmark).
- The instructions should contain the exact command and environment needed to run to reproduce the results. See the NeurIPS code and data submission guidelines (https://nips.cc/public/guides/CodeSubmissionPolicy) for more details.
- The authors should provide instructions on data access and preparation, including how
 to access the raw data, preprocessed data, intermediate data, and generated data, etc.
- The authors should provide scripts to reproduce all experimental results for the new proposed method and baselines. If only a subset of experiments are reproducible, they should state which ones are omitted from the script and why.
- At submission time, to preserve anonymity, the authors should release anonymized versions (if applicable).
- Providing as much information as possible in supplemental material (appended to the paper) is recommended, but including URLs to data and code is permitted.

6. Experimental setting/details

Question: Does the paper specify all the training and test details (e.g., data splits, hyperparameters, how they were chosen, type of optimizer, etc.) necessary to understand the results?

Answer: [Yes]

Justification: Detailed training specifications are provided in Appendix B.

Guidelines:

- The answer NA means that the paper does not include experiments.
- The experimental setting should be presented in the core of the paper to a level of detail that is necessary to appreciate the results and make sense of them.
- The full details can be provided either with the code, in appendix, or as supplemental material.

7. Experiment statistical significance

Question: Does the paper report error bars suitably and correctly defined or other appropriate information about the statistical significance of the experiments?

Answer: [Yes]

Justification: The figures and tables in this paper are primarily evaluated using the mean squared error (MSE) metric, with additional data from alternative error assessment methods provided.

- The answer NA means that the paper does not include experiments.
- The authors should answer "Yes" if the results are accompanied by error bars, confidence intervals, or statistical significance tests, at least for the experiments that support the main claims of the paper.

- The factors of variability that the error bars are capturing should be clearly stated (for example, train/test split, initialization, random drawing of some parameter, or overall run with given experimental conditions).
- The method for calculating the error bars should be explained (closed form formula, call to a library function, bootstrap, etc.)
- The assumptions made should be given (e.g., Normally distributed errors).
- It should be clear whether the error bar is the standard deviation or the standard error
 of the mean.
- It is OK to report 1-sigma error bars, but one should state it. The authors should preferably report a 2-sigma error bar than state that they have a 96% CI, if the hypothesis of Normality of errors is not verified.
- For asymmetric distributions, the authors should be careful not to show in tables or figures symmetric error bars that would yield results that are out of range (e.g. negative error rates).
- If error bars are reported in tables or plots, The authors should explain in the text how they were calculated and reference the corresponding figures or tables in the text.

8. Experiments compute resources

Question: For each experiment, does the paper provide sufficient information on the computer resources (type of compute workers, memory, time of execution) needed to reproduce the experiments?

Answer: [Yes]

Justification: Section 4 documents the machine learning frameworks and hardware configurations utilized in this work.

Guidelines:

- The answer NA means that the paper does not include experiments.
- The paper should indicate the type of compute workers CPU or GPU, internal cluster, or cloud provider, including relevant memory and storage.
- The paper should provide the amount of compute required for each of the individual experimental runs as well as estimate the total compute.
- The paper should disclose whether the full research project required more compute than the experiments reported in the paper (e.g., preliminary or failed experiments that didn't make it into the paper).

9. Code of ethics

Question: Does the research conducted in the paper conform, in every respect, with the NeurIPS Code of Ethics https://neurips.cc/public/EthicsGuidelines?

Answer: [Yes]

Justification: We have strictly followed the NeurIPS Code of Ethics.

Guidelines:

- The answer NA means that the authors have not reviewed the NeurIPS Code of Ethics.
- If the authors answer No, they should explain the special circumstances that require a
 deviation from the Code of Ethics.
- The authors should make sure to preserve anonymity (e.g., if there is a special consideration due to laws or regulations in their jurisdiction).

10. Broader impacts

Question: Does the paper discuss both potential positive societal impacts and negative societal impacts of the work performed?

Answer: [Yes]

Justification: Our work provides a positive contribution to the advancement of Physics-Informed Neural Networks (PINNs), while potential negative societal impacts are deemed negligible given the fundamental methodological focus and current scope of application.

- The answer NA means that there is no societal impact of the work performed.
- If the authors answer NA or No, they should explain why their work has no societal impact or why the paper does not address societal impact.
- Examples of negative societal impacts include potential malicious or unintended uses (e.g., disinformation, generating fake profiles, surveillance), fairness considerations (e.g., deployment of technologies that could make decisions that unfairly impact specific groups), privacy considerations, and security considerations.
- The conference expects that many papers will be foundational research and not tied to particular applications, let alone deployments. However, if there is a direct path to any negative applications, the authors should point it out. For example, it is legitimate to point out that an improvement in the quality of generative models could be used to generate deepfakes for disinformation. On the other hand, it is not needed to point out that a generic algorithm for optimizing neural networks could enable people to train models that generate Deepfakes faster.
- The authors should consider possible harms that could arise when the technology is being used as intended and functioning correctly, harms that could arise when the technology is being used as intended but gives incorrect results, and harms following from (intentional or unintentional) misuse of the technology.
- If there are negative societal impacts, the authors could also discuss possible mitigation strategies (e.g., gated release of models, providing defenses in addition to attacks, mechanisms for monitoring misuse, mechanisms to monitor how a system learns from feedback over time, improving the efficiency and accessibility of ML).

11. Safeguards

Question: Does the paper describe safeguards that have been put in place for responsible release of data or models that have a high risk for misuse (e.g., pretrained language models, image generators, or scraped datasets)?

Answer: [NA]

Justification: the paper poses no such risks.

Guidelines:

- The answer NA means that the paper poses no such risks.
- Released models that have a high risk for misuse or dual-use should be released with
 necessary safeguards to allow for controlled use of the model, for example by requiring
 that users adhere to usage guidelines or restrictions to access the model or implementing
 safety filters.
- Datasets that have been scraped from the Internet could pose safety risks. The authors should describe how they avoided releasing unsafe images.
- We recognize that providing effective safeguards is challenging, and many papers do not require this, but we encourage authors to take this into account and make a best faith effort.

12. Licenses for existing assets

Question: Are the creators or original owners of assets (e.g., code, data, models), used in the paper, properly credited and are the license and terms of use explicitly mentioned and properly respected?

Answer: [Yes]

Justification: All methodologies are accompanied by proper citations.

- The answer NA means that the paper does not use existing assets.
- The authors should cite the original paper that produced the code package or dataset.
- The authors should state which version of the asset is used and, if possible, include a URL.
- The name of the license (e.g., CC-BY 4.0) should be included for each asset.
- For scraped data from a particular source (e.g., website), the copyright and terms of service of that source should be provided.

- If assets are released, the license, copyright information, and terms of use in the
 package should be provided. For popular datasets, paperswithcode.com/datasets
 has curated licenses for some datasets. Their licensing guide can help determine the
 license of a dataset.
- For existing datasets that are re-packaged, both the original license and the license of the derived asset (if it has changed) should be provided.
- If this information is not available online, the authors are encouraged to reach out to the asset's creators.

13. New assets

Question: Are new assets introduced in the paper well documented and is the documentation provided alongside the assets?

Answer: [NA]

Justification: The paper does not release new assets.

Guidelines:

- The answer NA means that the paper does not release new assets.
- Researchers should communicate the details of the dataset/code/model as part of their submissions via structured templates. This includes details about training, license, limitations, etc.
- The paper should discuss whether and how consent was obtained from people whose asset is used.
- At submission time, remember to anonymize your assets (if applicable). You can either create an anonymized URL or include an anonymized zip file.

14. Crowdsourcing and research with human subjects

Question: For crowdsourcing experiments and research with human subjects, does the paper include the full text of instructions given to participants and screenshots, if applicable, as well as details about compensation (if any)?

Answer: [NA]

Justification: The paper does not involve crowdsourcing or research with human subjects.

Guidelines:

- The answer NA means that the paper does not involve crowdsourcing nor research with human subjects.
- Including this information in the supplemental material is fine, but if the main contribution of the paper involves human subjects, then as much detail as possible should be included in the main paper.
- According to the NeurIPS Code of Ethics, workers involved in data collection, curation, or other labor should be paid at least the minimum wage in the country of the data collector.

15. Institutional review board (IRB) approvals or equivalent for research with human subjects

Question: Does the paper describe potential risks incurred by study participants, whether such risks were disclosed to the subjects, and whether Institutional Review Board (IRB) approvals (or an equivalent approval/review based on the requirements of your country or institution) were obtained?

Answer: [NA]

Justification: The paper does not involve crowdsourcing nor research with human subjects. Guidelines:

- The answer NA means that the paper does not involve crowdsourcing nor research with human subjects.
- Depending on the country in which research is conducted, IRB approval (or equivalent) may be required for any human subjects research. If you obtained IRB approval, you should clearly state this in the paper.

- We recognize that the procedures for this may vary significantly between institutions and locations, and we expect authors to adhere to the NeurIPS Code of Ethics and the guidelines for their institution.
- For initial submissions, do not include any information that would break anonymity (if applicable), such as the institution conducting the review.

16. Declaration of LLM usage

Question: Does the paper describe the usage of LLMs if it is an important, original, or non-standard component of the core methods in this research? Note that if the LLM is used only for writing, editing, or formatting purposes and does not impact the core methodology, scientific rigorousness, or originality of the research, declaration is not required.

Answer: [NA]

Justification: The core method development in this research does not involve LLMs as any important, original, or non-standard components.

- The answer NA means that the core method development in this research does not involve LLMs as any important, original, or non-standard components.
- Please refer to our LLM policy (https://neurips.cc/Conferences/2025/LLM) for what should or should not be described.

A Supplementary Geometric Details

A.1 Case1:Flow around a Cylinder

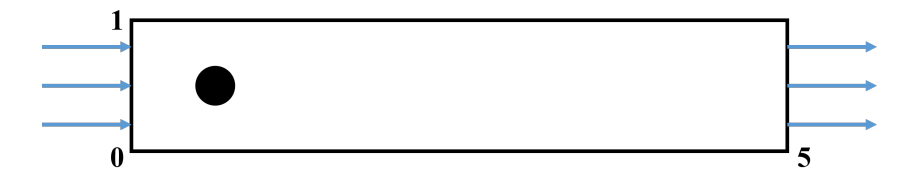


Figure 11: Scheme of the two-dimensional flow around a cylinder.

Case 1 corresponds to the canonical flow past a circular cylinder. As schematically depicted in Fig.11. Following non-dimensionalization, the computational domain is configured with a length of 5 and a width of 1. A circular obstruction with diameter D=0.2 is centered at (x,y)=(0.5,0.5). The boundary conditions are defined as follows:

- Inlet (Left Boundary): Horizontal inflow velocity u = 1, v = 0.
- Outlet (Right Boundary): Static pressure fixed at p = 0.
- Top/Bottom Boundaries: No-slip walls (u = v = 0).

This configuration corresponds to a Reynolds number Re=100, with the dimensionless density $\rho=1$. The dynamic viscosity ν is determined by the Reynolds number formula $Re=\frac{uD}{\nu}$, where u denotes the characteristic velocity and D the characteristic length.

A.2 Case2:Steady-State Flow in a Segmented Inlet with an Obstructed Square Cavity

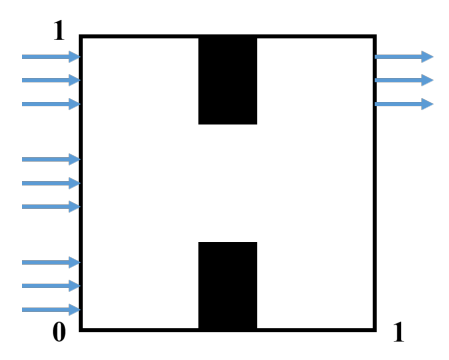


Figure 12: Scheme of the Segmented inlet with obstructed square cavity flow.

The model features two rectangular obstructions positioned at the top and bottom walls of a square cavity with an edge length of 1 unit. As illustrated in Fig.12, the inlet is divided into three segments, and the obstructions have a width of 0.2 units and a height of 0.3 units. The boundary conditions are defined as follows:

- Inlet: Normal inflow velocity u = 0.5, v = 0.
- Outlet: Static pressure set to p = 0.
- Other Boundaries: No-slip conditions (u = v = 0) on all walls and obstruction surfaces.

In Case 3 of the main text, the geometric configuration remains identical to that of Case 2, with the sole distinction lying in the incorporation of transient flow dynamics.

B Training Details

The framework is developed on the PyTorch machine learning platform, and training iterations are accelerated using a high-performance GPU.

B.1 Case1

Subnetwork $\mathcal{N}_{\mathcal{P}}$:

- Network architecture: Three separate deep neural networks (DNNs) for variables u, v, and p, each structured as $[2] + 6 \times [64] + [1]$
- Training epochs: 10,000
- · Activation function: tanh
- Optimizer: Adam
- Learning rate: 1×10^{-3}

Subnetwork $\mathcal{N}_{\mathcal{D}}$:

- Network architecture: Three separate DNNs for u, v, and p, each structured as $[2] + 4 \times [20] + [1]$
- Training epochs: 300,000
- · Activation function: tanh
- Optimizer: Adam
- Learning rate: Initial learning rate of 1×10^{-3} with a learning rate annealing strategy
- $\alpha = 10$

Subnetwork $\mathcal{N}_{\mathcal{H}}$:

- Network architecture: Three separate DNNs for u, v, and p, each structured as $[2]+6\times[128]+[1]$
- Training epochs: 300,000
- Activation function: tanh
- · Optimizer: Adam
- Learning rate: Initial learning rate of 1×10^{-3} with a learning rate annealing strategy

B.2 Case2

Subnetwork $\mathcal{N}_{\mathcal{P}}$:

- Network architecture: Three separate deep neural networks (DNNs) for variables u, v, and p, each structured as $[2] + 6 \times [64] + [1]$
- Training epochs: 10,000
- · Activation function: tanh
- Optimizer: Adam
- Learning rate: 1×10^{-3}

Subnetwork $\mathcal{N}_{\mathcal{D}}$:

- Network architecture: Three separate DNNs for u, v, and p, each structured as $[2] + 4 \times [64] + [1]$
- Training epochs: 300,000
- Activation function: tanh
- · Optimizer: Adam
- Learning rate: Initial learning rate of 1×10^{-3} with a learning rate annealing strategy
- $\alpha = 5$

Subnetwork $\mathcal{N}_{\mathcal{H}}$:

• Network architecture: Three separate DNNs for u, v, and p, each structured as $[2]+6\times[128]+[1]$

Training epochs: 500,000Activation function: tanh

• Optimizer: Adam

• Learning rate: Initial learning rate of 1×10^{-3} with a learning rate annealing strategy

B.3 Case3

Subnetwork $\mathcal{N}_{\mathcal{P}}$:

• Network architecture: Three separate deep neural networks (DNNs) for variables u, v, and p, each structured as $[3] + 6 \times [64] + [1]$

Training epochs: 10,000Activation function: tanhOptimizer: Adam

• Learning rate: 1×10^{-3}

Subnetwork $\mathcal{N}_{\mathcal{D}}$:

• Network architecture: Three separate DNNs for u, v, and p, each structured as $[3] + 4 \times [64] + [1]$

• Training epochs: 300,000

• Activation function: tanh

• Optimizer: Adam

• Learning rate: Initial learning rate of 1×10^{-3} with a learning rate annealing strategy

• $\alpha = 5$

Subnetwork $\mathcal{N}_{\mathcal{H}}$:

• Network architecture: Three separate DNNs for u, v, and p, each structured as $[3]+6\times[128]+[1]$

• Training epochs: 500,000

• Activation function: tanh

• Optimizer: Adam

• Learning rate: Initial learning rate of 1×10^{-3} with a learning rate annealing strategy

B.4 Other PINN methods

• Network architecture: Three separate DNNs for u, v, and p, each structured as $[2]+6\times[128]+[1]$

Training epochs: 500,000Activation function: tanh

• Optimizer: Adam

• Learning rate: Initial learning rate of 1×10^{-3} with a learning rate annealing strategy

• Points per epoch: 20,000 (random sampling from domain)

C Ablation studies

The three ablation studies are as follows:

1. Comparative analysis of mP (particular solution network only) and mD (distance metric network only) against hPINN and HB-PINN, where mP and mD represent experimental configurations using isolated components of HB-PINN.

- 2. Impact assessment of varying pre-training epochs for the particular solution network $(\mathcal{N}_{\mathcal{P}})$ on the final accuracy of the primary network.
- 3. Sensitivity analysis of the power-law exponent α in the distance metric network $(\mathcal{N}_{\mathcal{D}})$, which governs the transition steepness of the distance function, to evaluate its influence on solution accuracy.

C.1 mP and mD

In this section, we evaluate the outcomes of separately employing the particular solution network and the distance metric network, where mP refers to using only the particular solution network and mD refers to using only the distance metric network. The experimental results are compared with hPINN and HB-PINN, and velocity predictions are shown in Fig.13.

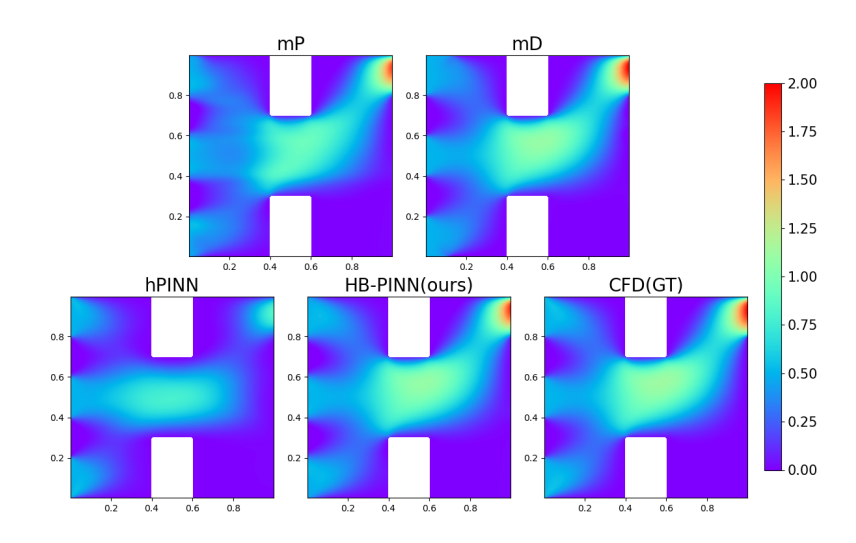


Figure 13: Comparison of velocity results of the mP and mD methods in Case 2.

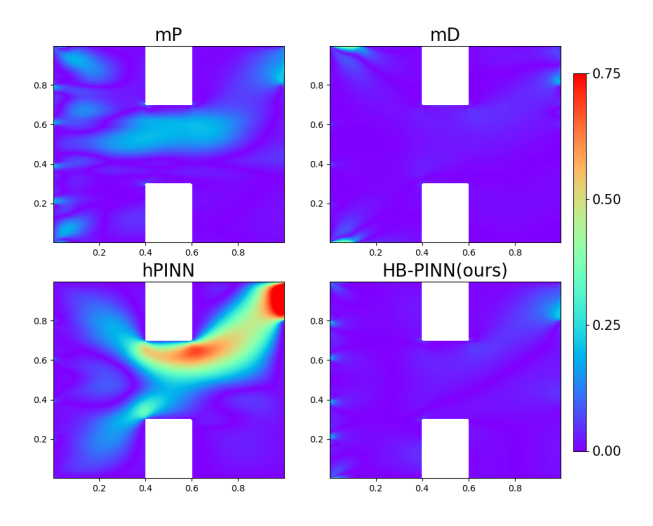


Figure 14: The residuals of mP, mD, hPINN, and HB-PINN compared to the GT in Case 2.

Under the mP approach, the distance function is normalized solely based on the distance to the boundary without adjustment using power functions, resulting in lower accuracy within the domain.

Under the mD approach, while internal errors are reduced during training, the enforcement of boundary conditions is imprecise, which affects the final results. These tests demonstrate that both constructive functions in our method contribute positively to the solution process, further validating the necessity of applying both functions simultaneously. The comparison of residuals is shown in Fig.14.More detailed error metrics are summarized in the "mP and mD" section of Table ??.

C.2 Particular solution network under different training epochs

In the HB-PINN method, the particular solution network $(\mathcal{N}_{\mathcal{P}})$ is trained with a shallow deep neural network (DNN) using a soft constraint approach, aiming to provide a pre-trained solution that satisfies the boundary conditions, by tuning the weights associated with the loss terms, the network's output is rigorously constrained to strictly satisfy the boundary conditions. When the weight of the boundary condition loss term in the loss function is set to an extremely high value (e.g., 1000), excessive training iterations may lead to overfitting in local boundary regions, thereby compromising the global smoothness of the network's output. To mitigate this issue, a strategy with limited training iterations is generally adopted. In this section, we supplement our analysis by investigating the impact of different training iterations (10,000, 30,000, and 50,000) of $\mathcal{N}_{\mathcal{P}}$ on the final training results. The velocity results and their residuals relative to the CFD method are shown in Fig.15,16.

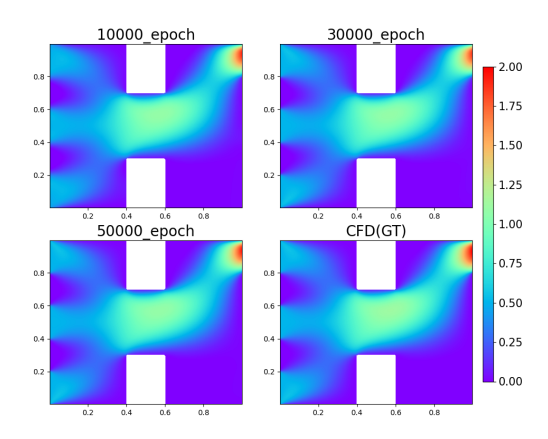


Figure 15: Final velocity results for $\mathcal{N}_{\mathcal{P}}$ trained with 10,000, 30,000, and 50,000 iterations.

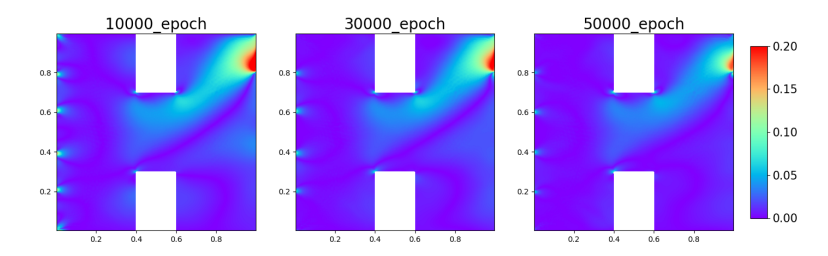


Figure 16: Residuals of the final velocity results compared to the CFD method for $\mathcal{N}_{\mathcal{P}}$ trained with 10,000, 30,000, and 50,000 iterations.

As evidenced by the error metrics in Figure 15 and the "Epoch for $\mathcal{N}_{\mathcal{P}}$ " section of Table 2, limiting the training iterations of the particular solution subnetwork $(\mathcal{N}_{\mathcal{P}})$ leads to lower global error within the computational domain and more rapid convergence of the primary network $(\mathcal{N}_{\mathcal{H}})$. However, this configuration results in reduced precision in boundary regions compared to cases where $\mathcal{N}_{\mathcal{P}}$ undergoes extended training. Currently, the number of training iterations for $\mathcal{N}_{\mathcal{P}}$ is determined empirically, and further research is needed to balance accuracy and convergence speed optimally.

C.3 Distance metric network under different α

This section evaluates the impact of four critical parameter values ($\alpha=3,5,10,15$) in the distance metric network on the predictive performance of the HB-PINN method. Notably, $\alpha=5$ corresponds to the parameter configuration adopted in Case 2 of the main text. The velocity prediction results, as illustrated in Fig.17, demonstrate the sensitivity of model accuracy to variations in α .

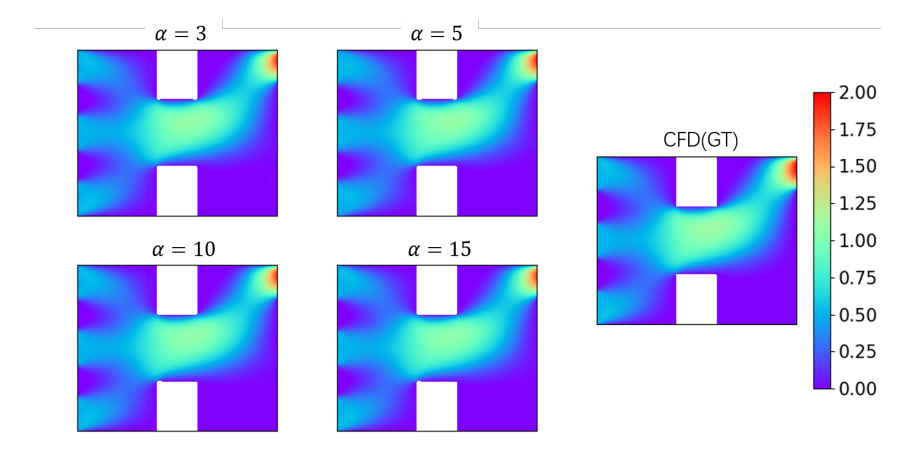


Figure 17: Comparison of velocity results between HB-PINN and CFD for $\alpha = 3, 5, 10$, and 15.

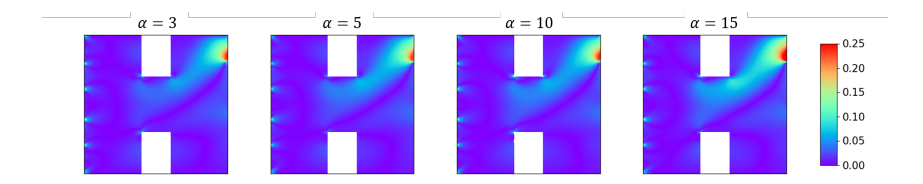


Figure 18: Residuals between HB-PINN and CFD velocity results for $\alpha = 3, 5, 10$, and 15.

The parameter α governs the steepness of the transition in the distance function near boundaries. Excessively small α values (e.g., $\alpha=3$) result in insufficient sensitivity to boundary constraints, while overly large α values (e.g., $\alpha=10,15$) lead to excessively thin boundary layers, thereby amplifying training challenges in boundary regions. The velocity prediction residuals compared to CFD results and the statistical metrics of the mean squared error (MSE) are shown in Fig.18 and the α for $\mathcal{N}_{\mathcal{D}}$ section of Table2. These results indicate that both undersized and oversized α values degrade prediction accuracy. However, the selection of α currently remains empirically determined, and identifying an optimal α value warrants further investigation.

C.4 Error Records

D Supplementary Details on Boundary Condition Relaxation in the hPINN Method

In the hPINN method, using only boundary conditions to constrain the solution network $\mathcal{N}_{\mathcal{P}}$ is effective when the boundary conditions are simple. However, for complex boundaries, this approach leads to distorted or discontinuous outputs within the solution domain, especially near junctions between different boundary types.

Fig.19 presents the results of the boundary particular solution network $\mathcal{N}_{\mathcal{P}}$ from the original hPINN, the hPINN with partially relaxed boundary constraints, and the HB-PINN. It can be clearly observed that under the original hPINN framework, the output of the $\mathcal{N}_{\mathcal{P}}$ network exhibits irregular solutions within the domain. Since it is trained solely on boundary conditions, its internal results are uncontrollable. This significantly increases the training difficulty of the main network, even hindering

Table 2: Comparative analysis of error metrics across ablation studies

Category	Configuration	Error Metrics(↓)		
		MSE(↓)	MAE(↓)	Relative L2(↓)
	hPINN	0.04060	0.11242	0.45110
mP & mD	mP	0.00484	0.04589	0.15575
IIIP & IIID	mD	0.00409	0.02269	0.14329
	HB-PINN	0.00088	0.01888	0.06655
	10000	0.00088	0.01888	0.06655
Epoch for $\mathcal{N}_{\mathcal{P}}$	30000	0.00234	0.01907	0.10833
_	50000	0.00248	0.01644	0.11169
	3	0.00471	0.02577	0.15374
o for M	5	0.00088	0.01888	0.06655
α for $\mathcal{N}_{\mathcal{D}}$	10	0.00177	0.02312	0.09429
	15	0.00140	0.02199	0.08403

convergence – as we observed in our hPINN experiments: strict constraints on certain boundary regions had to be relaxed for the main network loss to decrease effectively. The loss records in Table3 fully demonstrate this point. In Relaxed hPINN, we relaxed the boundary constraints in the regions 0 < x < 0.4, y = 0 & y = 1, which indeed effectively promoted the reduction of loss during main network training. However, this compromise violates the requirement for full boundary condition satisfaction, which is unacceptable for solving physical models. This precisely highlights the dilemma of traditional hard-constraint methods when handling complex boundary problems. Therefore, we introduced the $\mathcal{N}_{\mathcal{P}}$ with weak equation constraints as an alternative solution aimed at more robustly handling complex boundary constraints.

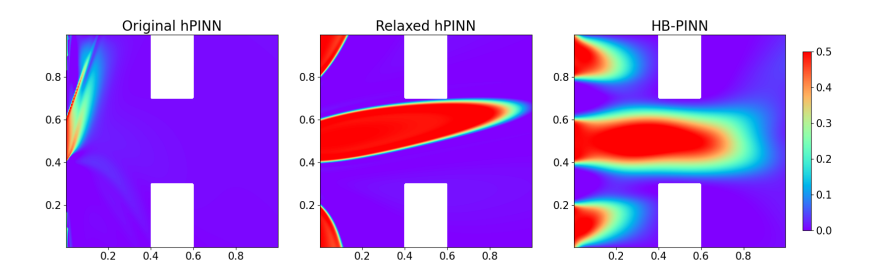


Figure 19: Comparative Analysis of Particular Solution Network Results across Original hPINN, Relaxed hPINN, and HB-PINN

Table 3: Loss comparison across different methods at various epochs

Epoch	Original hPINN	Relaxed hPINN	HB-PINN
0	2335810	47.44	7.129
1000	15292	29.82	2.517
2000	1855618	30.75	1.797
3000	5720168	28.45	1.588

E Supplementary details of the transient case (Case 3).

In the main text of Case 3, we present the velocity results at t = 1 for the transient segmented inlet with obstructed square cavity flow model. At t = 1, the flow can be considered to have developed to a state approaching steady-state results. Fig.20,21,22,23 display the velocity results at several time

steps during the development of the transient model, specifically at t = 0.1, t = 0.3, t = 0.5, and t = 0.7, to demonstrate that our HB-PINN method achieves high accuracy across all time steps when solving the transient model. The errors in velocity relative to the CFD method are shown in Fig.24,25,26,27

The velocity results at different time steps and their corresponding mean square errors relative to the CFD method are quantitatively summarized in Table4.

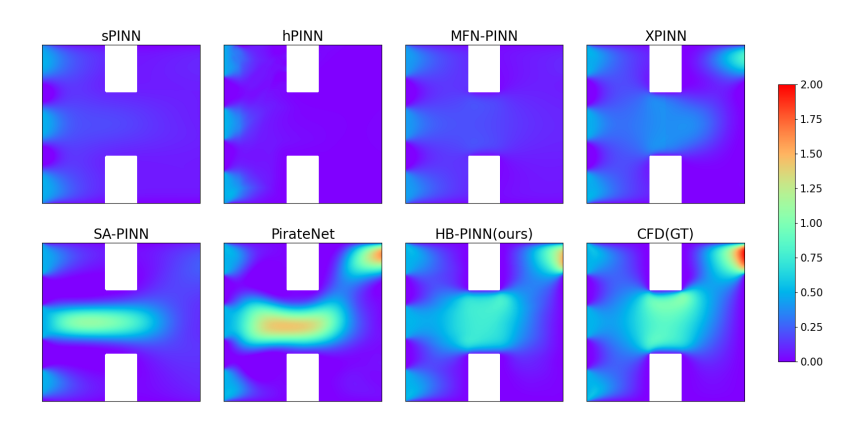


Figure 20: Comparison of velocity distributions at t = 0.1 for different methods in Case 3.

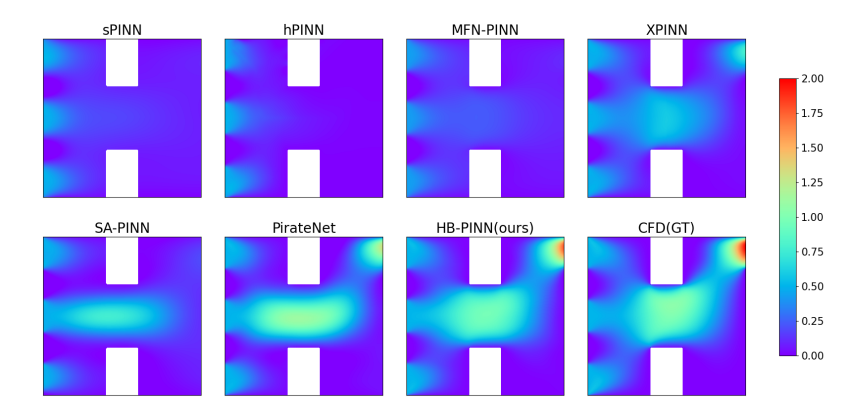


Figure 21: Comparison of velocity distributions at t = 0.3 for different methods in Case 3.

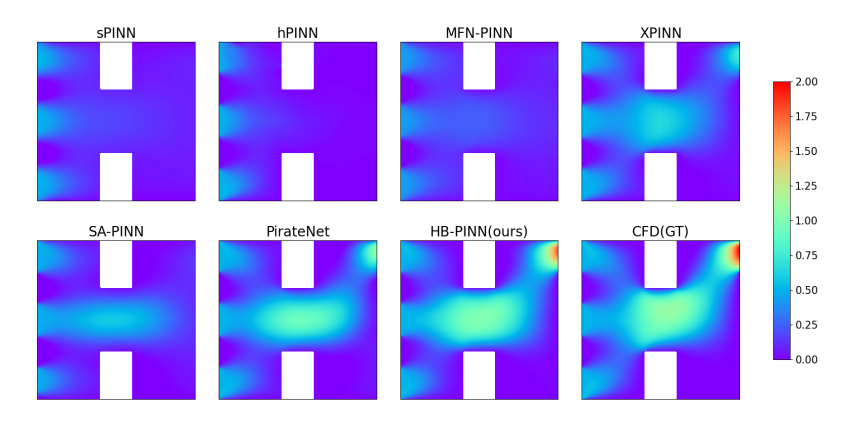


Figure 22: Comparison of velocity distributions at t = 0.5 for different methods in Case 3.

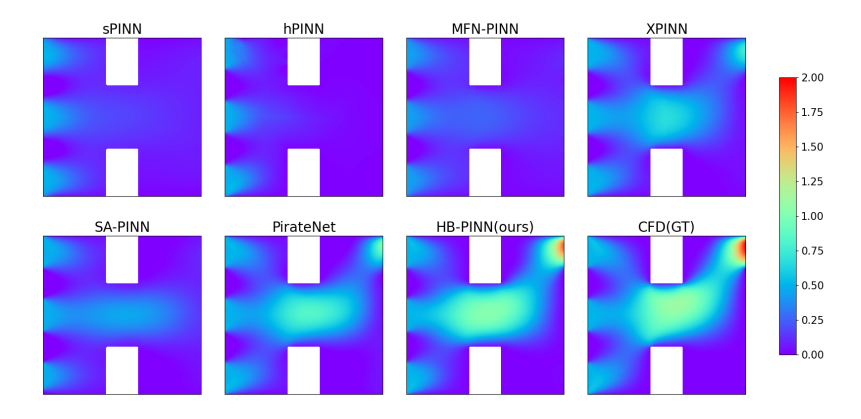


Figure 23: Comparison of velocity distributions at t = 0.7 for different methods in Case 3.

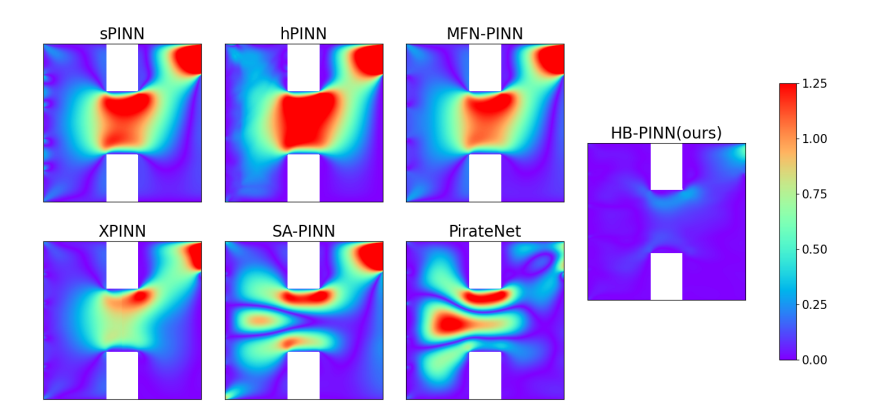


Figure 24: Comparison of the residuals relative to the ground truth (GT) for sPINN, hPINN, SA-PINN, XPINN, and our HB-PINN at t = 0.1 in Case 3.

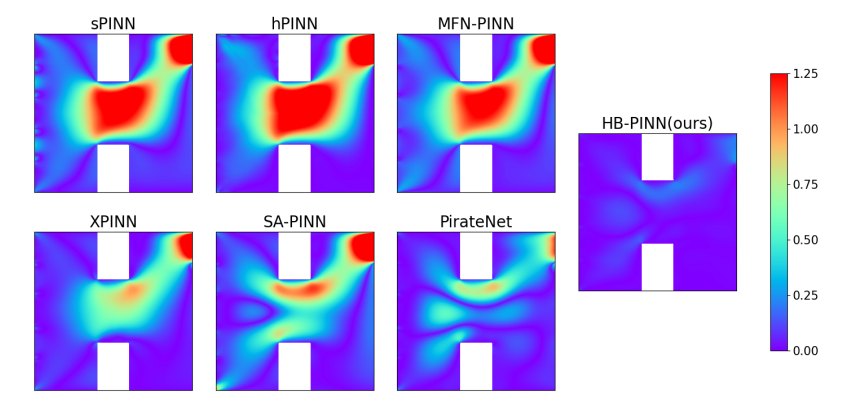


Figure 25: Comparison of the residuals relative to the ground truth (GT) for sPINN, hPINN, SA-PINN, XPINN, and our HB-PINN at t = 0.3 in Case 3.

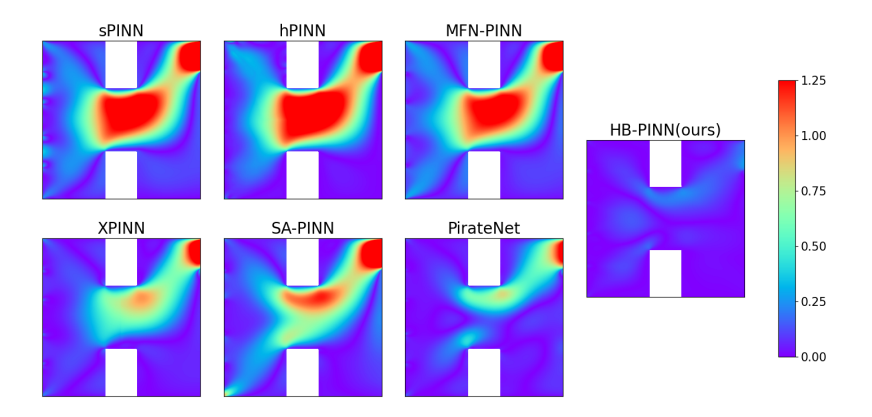


Figure 26: Comparison of the residuals relative to the ground truth (GT) for sPINN, hPINN, SA-PINN, XPINN, and our HB-PINN at t = 0.5 in Case 3.

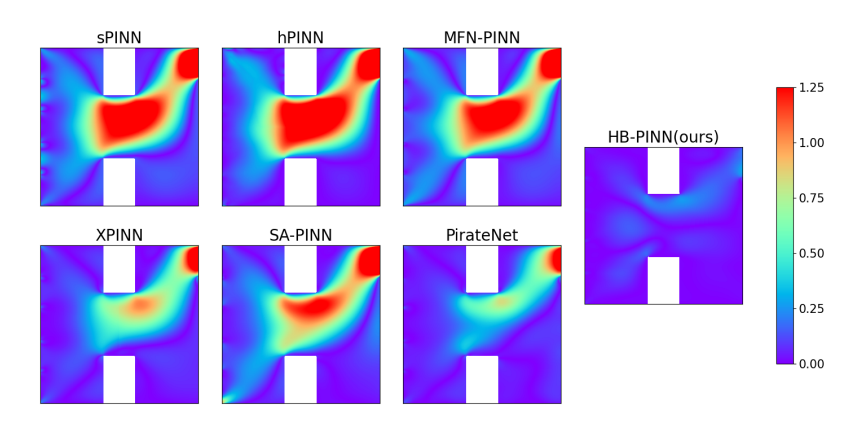


Figure 27: Comparison of the residuals relative to the ground truth (GT) for sPINN, hPINN, SA-PINN, XPINN, and our HB-PINN at t = 0.7 in Case 3.

F Cross-sectional profiles and time-history results in high-gradient regions

This section compares the velocity and pressure predictions of sPINN, PirateNet, and HB-PINN in high-gradient regions. Fig.28 displays the predictive results along the cross-section at y=0.5 in Case 2 compared with CFD results, while Fig.29 presents the temporal distribution of predictions at the center point (0.5,0.5) in Case 3 against CFD references. Both regions represent areas with substantial gradients within their respective domains. The results demonstrate that HB-PINN achieves optimal prediction accuracy for all physical quantities in both test cases.

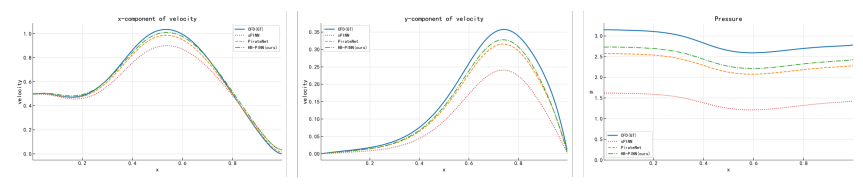


Figure 28: Comparison of velocity and pressure profiles along the y=0.5 cross-section in Case 2.

Table 4: Comparative analysis of error metrics across different methods at multiple time steps

Time	Method	Error Metrics				
		MSE(↓)	$\text{MAE}(\downarrow)$	Relative L2(\downarrow)		
	sPINN	0.11193	0.21171	0.78271		
	hPINN	0.16037	0.25855	0.93688		
	MFN-PINN	0.10544	0.20614	0.75967		
t = 0.1	XPINN	0.05466	0.15106	0.54699		
	SA-PINN	0.07638	0.17218	0.64659		
	PirateNet	0.05228	0.14450	0.53493		
	HB-PINN	0.00873	0.05070	0.21864		
	sPINN	0.11906	0.21625	0.788 15		
	hPINN	0.15441	0.24152	0.89754		
t = 0.3	MFN-PINN	0.10933	0.20813	0.75523		
	XPINN	0.04174	0.12288	0.46666		
	SA-PINN	0.06736	0.15283	0.59280		
	PirateNet	0.01989	0.09057	0.32215		
	HB-PINN	0.00580	0.04194	0.17405		
	sPINN	0.12218	0.21831	0.789 21		
	hPINN	0.15547	0.24054	0.89026		
	MFN-PINN	0.11164	0.20994	0.75441		
t = 0.5	XPINN	0.04046	0.11980	0.45416		
	SA-PINN	0.07700	0.16465	0.62653		
	PirateNet	0.02027	0.08035	0.32152		
	HB-PINN	0.00700	0.04895	0.18901		
	sPINN	0.12368	0.21927	0.78948		
	hPINN	0.15607	0.24033	0.88685		
	MFN-PINN	0.11283	0.21061	0.75405		
t = 0.7	XPINN	0.04087	0.11990	0.45383		
	SA-PINN	0.08956	0.17947	0.67181		
	PirateNet	0.02522	0.09204	0.35652		
	HB-PINN	0.00805	0.05228	0.20079		
	sPINN	0.12400	0.21876	0.78819		
	hPINN	0.15559	0.23951	0.88288		
	MFN-PINN	0.10543	0.20150	0.72678		
t = 1.0	XPINN	0.04149	0.12028	0.45592		
	SA-PINN	0.10612	0.19642	0.72915		
	PirateNet	0.03202	0.10682	0.40054		
	HB-PINN	0.00825	0.04870	0.20332		

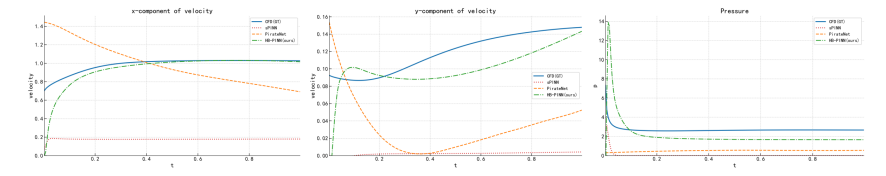


Figure 29: Comparison of Temporal Distributions of Velocity and Pressure at (0.5, 0.5) in Case 3.

G Steady-state flow in a square cavity with obstructed segmented inlet at different Reynolds numbers

As an extension of the comparative study on three flow models under the Reynolds number Re=100 scenario in the main text, this supplementary investigation systematically evaluates model

performance at elevated Reynolds numbers (Re = 500, 1000, 2000) using the Case 2 configuration, while strictly maintaining the original geometric structure and boundary conditions.

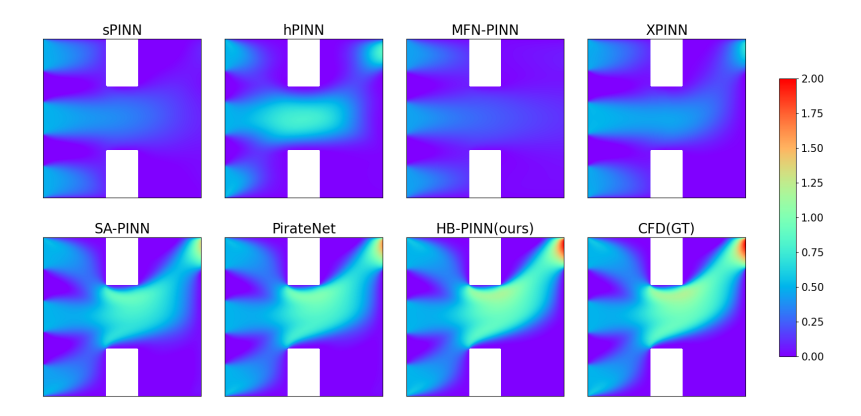


Figure 30: Comparison of velocity results under different methods for steady-state flow in a square cavity with obstructed segmented inlet at Reynolds number Re = 500.

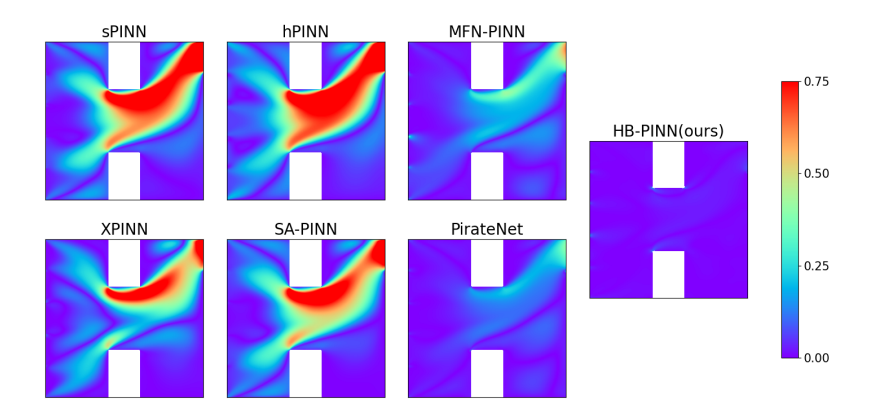


Figure 31: Comparison of velocity residuals relative to ground truth (GT) for steady-state flow in a square cavity with obstructed segmented inlet at Re=500, evaluated under different numerical methods.

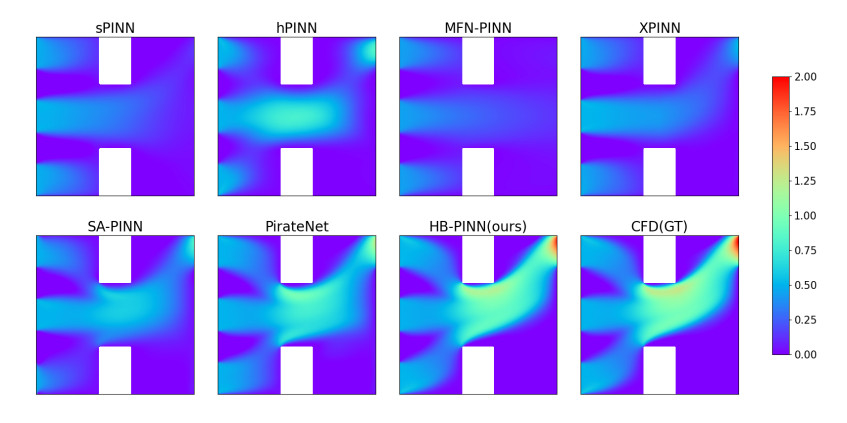


Figure 32: Comparison of velocity results under different methods for steady-state flow in a square cavity with obstructed segmented inlet at Reynolds number Re = 1000.

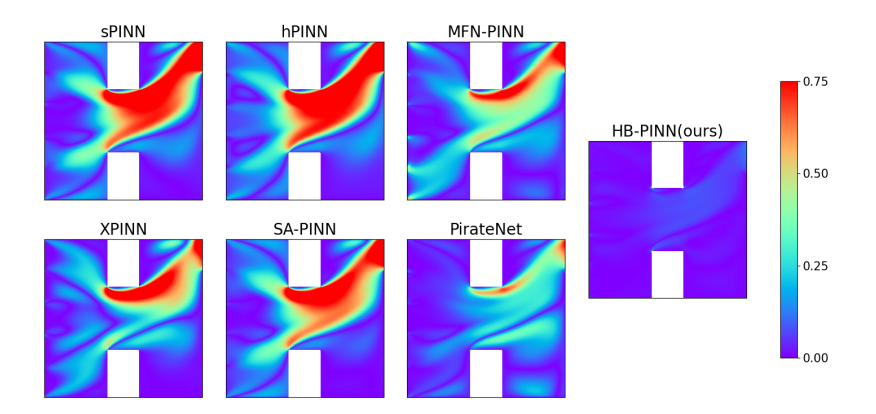


Figure 33: Comparison of velocity residuals relative to ground truth (GT) for steady-state flow in a square cavity with obstructed segmented inlet at Re=1000, evaluated under different numerical methods.

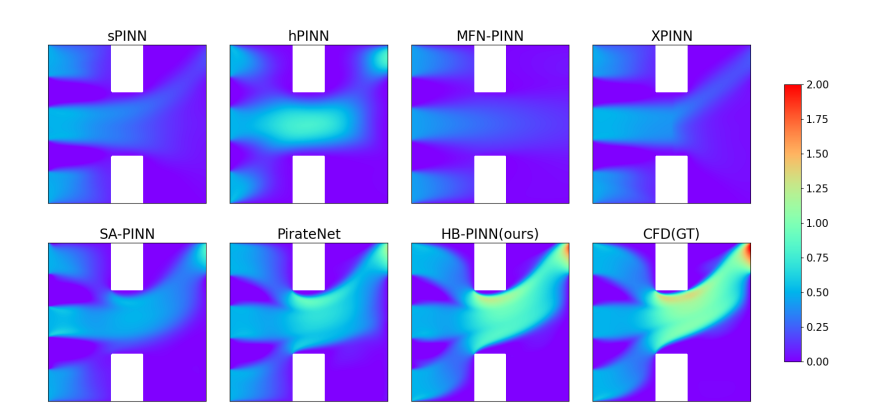


Figure 34: Comparison of velocity results under different methods for steady-state flow in a square cavity with obstructed segmented inlet at Reynolds number Re=2000.

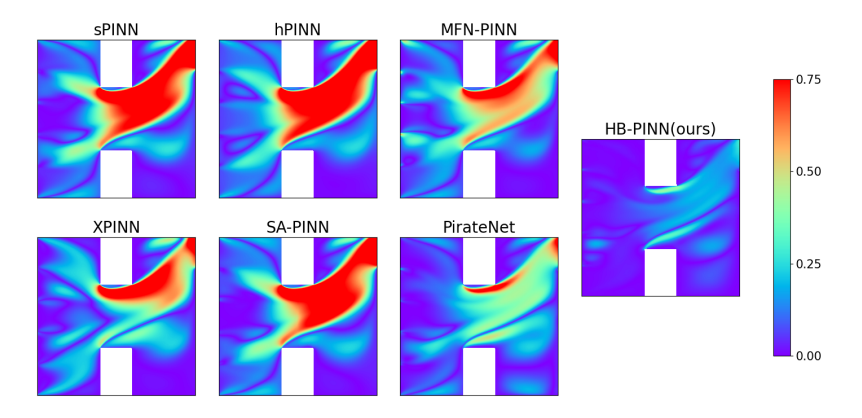


Figure 35: Comparison of velocity residuals relative to ground truth (GT) for steady-state flow in a square cavity with obstructed segmented inlet at Re=2000, evaluated under different numerical methods.

Fig.30,32,34 present the velocity predictions of different methods at Re = 500, 1000, and 2000, respectively, while their residuals relative to high-fidelity CFD results are visualized in Fig.31,33,35. As shown in the MSE variation trends across Reynolds numbers (Fig.36), all methods exhibit rising

prediction errors with increasing Re. However, the proposed HB-PINN consistently achieves the lowest MSE values at every Reynolds number.

Quantitative error metrics under multiple evaluation criteria are tabulated in Table.5. Notably, HB-PINN achieves an order-of-magnitude reduction in MSE compared to conventional methods at Re=500 and 1000. Even under the most challenging Re=2000 condition, HB-PINN demonstrates a notable accuracy improvement.

Table 5: Comparative analysis of error metrics across different methods under varying Reynolds numbers (Re).

Re	Method	Error Metrics			
	Wichiod	$\overline{\text{MSE}(\downarrow)}$	MAE(↓)	Relative L2(↓)	
	sPINN	0.11463	0.20569	0.74024	
	hPINN	0.05682	0.13910	0.52116	
	MFN-PINN	0.12693	0.22163	0.77892	
500	XPINN	0.08425	0.17904	0.63462	
	SA-PINN	0.01379	0.07827	0.25681	
	PirateNet	0.00591	0.05145	0.16819	
	HB-PINN	0.00071	0.01122	0.05865	
	sPINN	0.12541	0.21597	0.753 06	
	hPINN	0.06873	0.15608	0.55750	
	MFN-PINN	0.13945	0.23243	0.79408	
1000	XPINN	0.10250	0.19643	0.68079	
	SA-PINN	0.05881	0.15842	0.51569	
	PirateNet	0.02666	0.11171	0.34722	
	HB-PINN	0.00364	0.02857	0.12837	
	sPINN	0.13326	0.22616	0.75587	
2000	hPINN	0.08026	0.17093	0.58663	
	MFN-PINN	0.15202	0.24213	0.80734	
	XPINN	0.13156	0.22341	0.75103	
	SA-PINN	0.07584	0.17681	0.57022	
	PirateNet	0.04191	0.14184	0.42391	
	HB-PINN	0.02075	0.06640	0.29832	

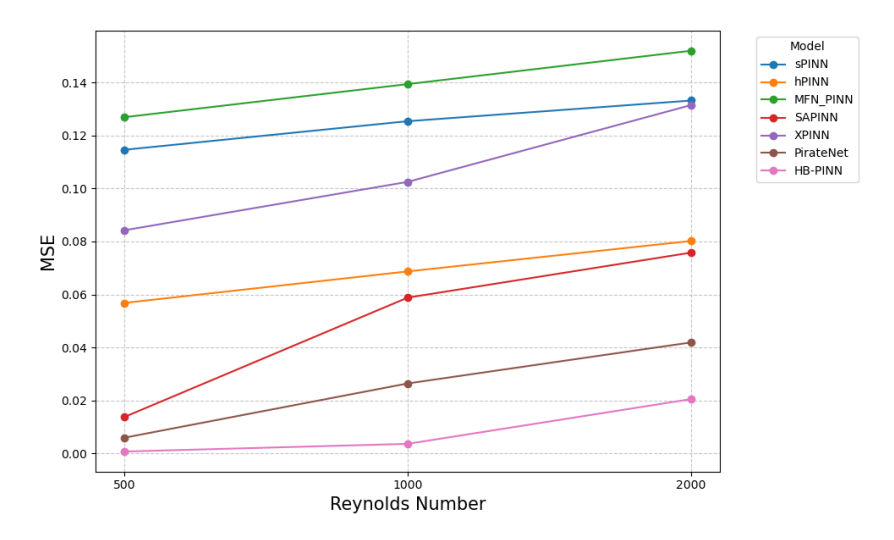


Figure 36: MSE Comparison with Reynolds Numbers

H The more complex obstructed cavity flow model

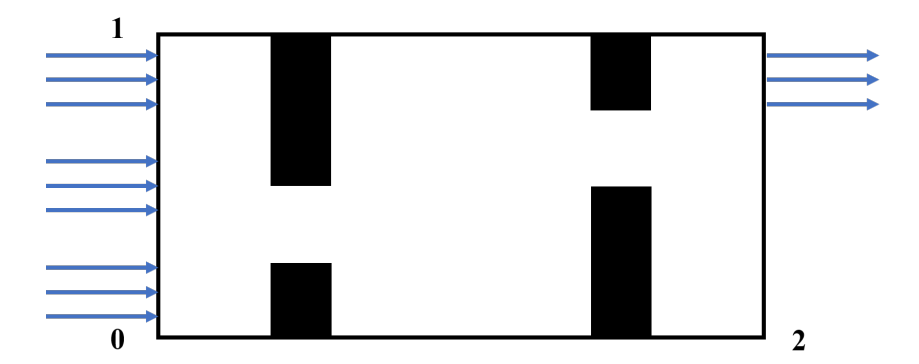


Figure 37: Extended schematic of the segmented inlet configuration in an obstructed rectangular cavity flow.

To validate the capability of our Hybrid Boundary Physics-Informed Neural Network (HB-PINN) in handling geometrically complex scenarios, we extend Case 2 from the main text to a more intricate configuration. As illustrated in Fig.37, the computational domain is expanded to a rectangular cavity of width 2 and height 1. Two types of staggered obstructions are embedded within the cavity:

- Type A Obstructions: Width = 0.2, Height = 0.5
- Type B Obstructions: Width = 0.2, Height = 0.25

The segmented inlet configuration (see Appendix E.1 for geometric specifics) imposes a normal inflow velocity u=0.5, while the outlet, positioned at the upper-right corner of the cavity, enforces a static pressure p=0. All other boundaries adhere to no-slip conditions (u=v=0).

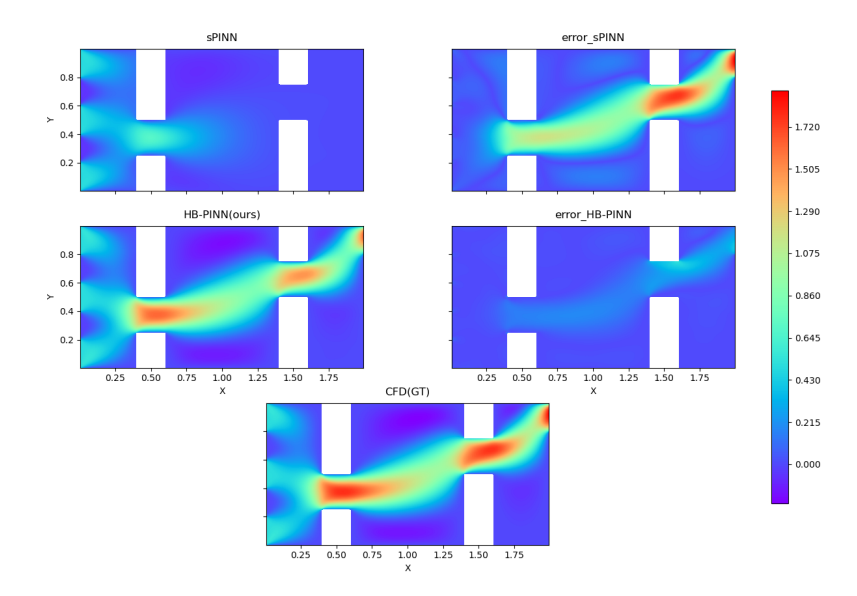


Figure 38: Velocity predictions and residuals of sPINN versus HB-PINN in the extended obstructed cavity flow model. Left: Velocity predictions; Right: Absolute errors relative to CFD; Bottom: CFD-computed results.

Fig.38 compares the velocity prediction results of conventional soft-constrained PINN (sPINN) and the proposed HB-PINN in the extended obstructed cavity flow model. As the geometric and physical

complexity of the model increases, traditional PINN methods struggle to resolve conflicts between competing loss terms (e.g., boundary condition residuals vs. governing equation residuals), leading to significant performance degradation in velocity field predictions. In contrast, HB-PINN maintains robust training convergence and achieves consistently accurate results. More detailed error metrics are summarized in the "Complex Cavity Flow" section of Table 6.

I Heat equation

To demonstrate the applicability of the HB-PINN method to other PDE systems, we evaluate its performance on a two-dimensional transient heat conduction problem, governed by the following equation:

$$\frac{\partial T}{\partial t} = \alpha \left(\frac{\partial^2 T}{\partial x^2} + \frac{\partial^2 T}{\partial y^2} \right),\tag{12}$$

T(x,y,t) represents the temperature field, where the thermal diffusivity $\alpha=\frac{k}{\rho c}$ is defined by the thermal conductivity k, density ρ , and specific heat capacity c. The geometric configuration, shown in Fig.39, features a square domain with edge length 1, containing four square heat sources (edge length 0.1) centered at coordinates (0.3,0.3), (0.3,0.7), (0.7,0.3), and (0.7,0.7). These heat sources are maintained at a dimensionless temperature of 1, while all external boundaries are fixed at 0.

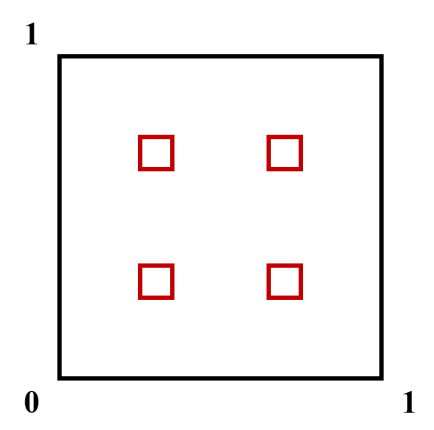


Figure 39: Geometric configurations employed in heat conduction problems

J Lid-driven Cavity flow

In this section, we evaluate the performance of HB-PINN in lid-driven cavity (LDC) flow, a classical benchmark problem in computational fluid dynamics. The LDC flow involves simulating the motion of an incompressible fluid within a two-dimensional square cavity, where the top lid is assigned a horizontal velocity of u=1, while the other walls maintain a no-slip condition. The boundary conditions are mathematically formulated as follows:

$$\begin{array}{lll} u=1, & 0\leq x\leq 1,\; y=1; & u=0, & \text{others;} \\ v=0, & \text{on } \partial\Omega; & p=0, & (0,0). \end{array}$$

The velocity predictions of sPINN and HB-PINN are shown in Fig.42. Due to the simpler geometric configuration of the model compared to the cases discussed in the main text, the improvement in accuracy is less pronounced than that observed in complex-boundary models. However, as evidenced by the residual results in Fig.43, HB-PINN exhibits significantly lower errors near boundaries. This finding aligns with the conclusions drawn in Appendix G, demonstrating that HB-PINN consistently achieves higher precision in boundary regions across diverse models. More detailed error metrics are summarized in the "LDC" section of Table 6.

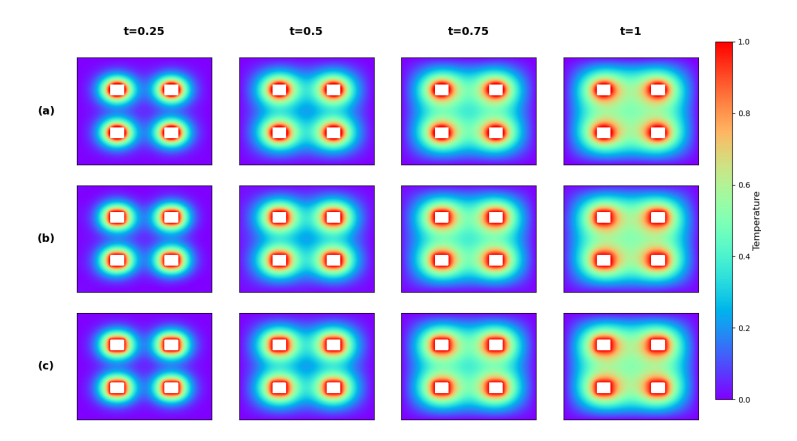


Figure 40: Comparison of temperature results at $t=0.25,\,0.5,\,0.75,\,$ and 1.0 for the heat conduction problem: (a) sPINN predictions; (b) HB-PINN predictions; (c) ground truth (GT).

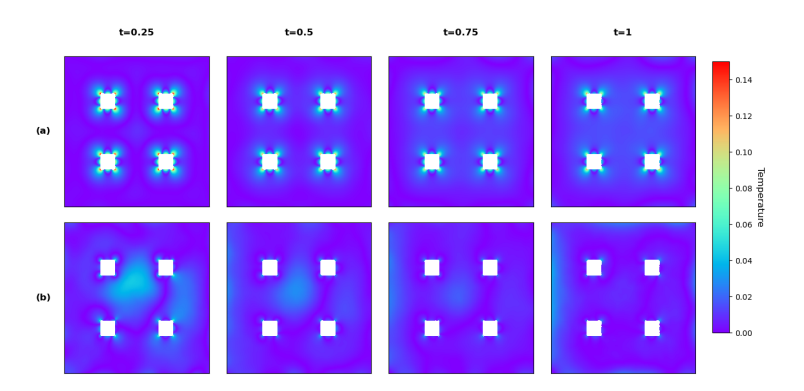


Figure 41: Residuals between predicted temperature and ground truth (GT) at $t=0.25,\,0.5,\,0.75,\,$ and 1.0 for the heat conduction problem: (a) Residuals of sPINN predictions;(b) Residuals of HB-PINN predictions.

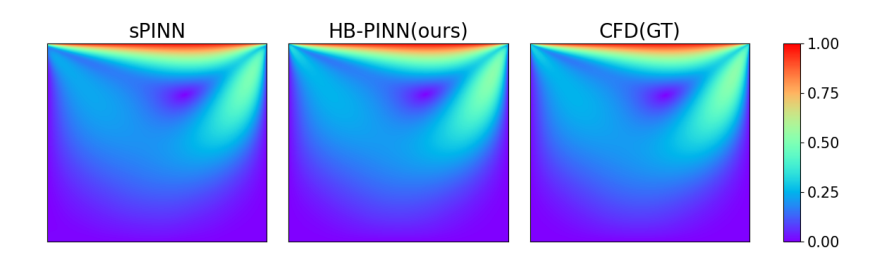


Figure 42: Comparison of Velocity Predictions Between sPINN, HB-PINN, and CFD in Lid-Driven Cavity Flow.

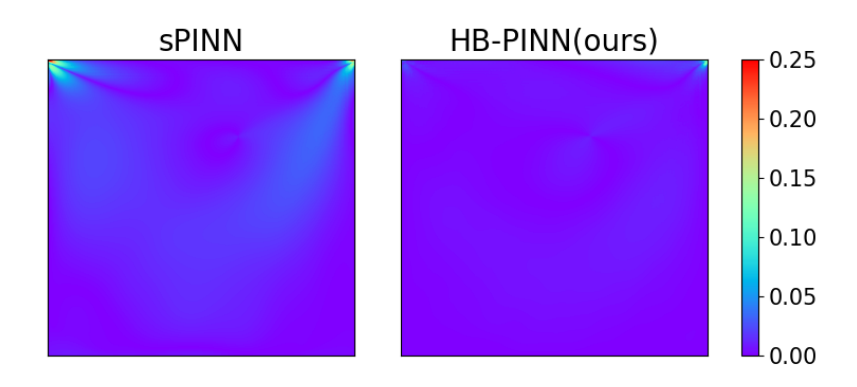


Figure 43: Residuals of Velocity Predictions Between sPINN, HB-PINN, and CFD in Lid-Driven Cavity Flow

Table 6: Comparative analysis of error metrics across the more complex obstructed cavity flow, heat equation, and Lid-Driven Cavity (LDC) flow

Problem	Method	Error Metrics		
110010111	1,10thou	MSE(↓)	MAE(↓)	Relative L2(\downarrow)
Complex Cavity Flow	sPINN	0.215 89	0.257 29	0.838 66
	HB-PINN	0.01331	0.05637	0.20829
Heat equation $(t = 1)$	sPINN	0.00276	0.017 80	0.10773
	HB-PINN	0.00090	0.01071	0.06152
LDC	sPINN	0.000 23	0.011 52	0.05873
	HB-PINN	0.00002	0.00377	0.02001

K Training and Inference Times

Table 7: Comparison of Training and Inference Times

Method	Training Time (1000 epochs)	Inference Time
SPINN	31.1 s	_
hPINN	48.3 s	_
MFN-PINN	92.5 s	_
XPINN	101.5 s	_
SA-PINN	41.4 s	_
PirateNet	106.9 s	_
HB-PINN	47.8 s	0.29 s
CFD	-	17 s